Research Square

Preprints are preliminary reports that have not undergone peer review.
They should not be considered conclusive, used to inform clinical practice,
or referenced by the media as validated information.

# Multi-Slotted Hexagonal-Core Resonant Architecture for an Ultra- Efficient Graphene THz MIMO Antenna with Exceptional Diversity for 6G Wireless Systems

**Saif Al Sahaf**
Daffodil International University
**Nafisa Anjum**
Daffodil International University
**Badhan Sarker**
Daffodil International University
**Jun-Jiat Tiang**
jjtiang@mmu.edu.my
Multimedia University
**Md Mostakim**
Daffodil International University
**Md Fokhrul Islam**
Daffodil International University
**Md. Ashraful Haque**
University of Liberal Arts Bangladesh (ULAB)

**Research Article**

**Keywords:** THz, Internet of Things (IoT), Single Element, MIMO Antenna, High Gain, Radiation Efficiency, RLC Equivalent Circuit, Industrial Applications and Innovation

**Posted Date:** November 18th, 2026

**DOI:** https://doi.org/10.21203/rs.3.rs-11518427/v1

**License:** This work is licensed under a Creative Commons Attribution 4.0 International License.
Read Full License

**Additional Declarations:** No competing interests reported.

# Multi-Slotted Hexagonal-Core Resonant Architecture for an Ultra-Efficient Graphene THz MIMO Antenna with Exceptional Diversity for 6G Wireless Systems.

**Saif Al Sahaf[1], Nafisa Anjum[1], Badhan Sarker[1], Jun-Jiat Tiang[2*], Md Mostakim[1], Md Fokhrul Islam[1], Md. Ashraful Haque[3*]**

[1]Department of Electrical and Electronic Engineering, Daffodil International University, Dhaka 1216, Bangladesh
[2]Centre for Wireless Technology, CoE for Intelligent Network, Faculty of Artificial Intelligence and Engineering, Multimedia University, Persiaran Multimedia, 63100, Cyberjaya, Selangor, Malaysia
[3]Department of Electrical and Electronic Engineering, University of Liberal Arts Bangladesh (ULAB), Dhaka, 1207, Bangladesh

Corresponding Authors: jjtiang@mmu.edu.my

**Abstract:**

This paper presents a low-profile graphene-based hexagonal-core resonator 1×2 multiple-input multiple-output (MIMO) antenna for future sixth-generation (6G) wireless communication systems operating in the terahertz (THz) band. The antenna consists of a graphene radiating patch on a flexible polyimide substrate with an annealed copper ground plane. The designed antenna is optimized by evolving its geometry while simultaneously optimizing the feed, substrate thickness, and ground thickness to improve impedance matching, gain, bandwidth, efficiency, isolation, and diversity performance. The patch resonates at 2.61, 3.50, 4.4531, and 6.25 THz, with impedance bandwidths of 0.6156, 0.7822, 0.815, and 1.5226 THz, respectively, and a reduced pattern of $1.827\lambda_o \times 0.783\lambda_o$. The antenna achieves a peak gain of 13.1076 dB and a radiating efficiency of 99.038%. The designed antenna achieves port isolation greater than −30.668 dB and −67.4517 dB due to its orthogonal, anti-parallel feeding configuration. The envelope correlation coefficient is found to be insignificant (0.012) and diversity gain is 10 dB which shows satisfactory MIMO multiplicity functionality. The graphene patch radiator is conductive enough for electricity, and the extensible polyimide base and reduced surface area for THz operation allows for a loss-free deployment. We created and verified an analogous RLC circuit for the designed antenna using CST full-wave and ADS circuit simulators. The simulation resonances match the proposed equivalent RLC circuit model well. The designed antenna can be used for 6G communication, THz sensing, imaging, spectroscopy, the Internet of Things (IoT), emerging industrial applications, and innovative wireless technologies. The electromagnetic and circuit-level simulations provide insight into the resonance mechanism, impedance behavior, and frequency-selective response.

**Keywords:** THz, Internet of Things (IoT), Single Element, MIMO Antenna, High Gain, Radiation Efficiency, RLC Equivalent Circuit, Industrial Applications and Innovation.

**Introduction:**

Sixth-generation (6G) communication systems primarily rely on terahertz (THz) antenna technology because it enables ultra-wide operational bandwidth, terabit-per-second data speeds, directional links, localization, and combined sensing and communication [1]. Millimeter-wave and sub-millimeter-wave communication systems enable compact implementation of ultra-massive antenna arrays for upcoming uses, including digital twins, extended reality, and holographic communications. Significant free-space attenuation, molecular absorption, blockage, beam misalignment, limited range, and technological flaws in existing THz devices, such as conductor and dielectric losses, are the primary obstacles to developing future THz communication systems [2]. As a result, THz antennas in 6G systems should be compact, beam-steering, wideband, high-efficiency, low-sidelobe, and high-gain. Advanced materials, graphene-based antennas, meta-surface-informed radiators, antenna-on-a-chip designs, very large MIMO systems, and sophisticated beamforming can help achieve the required performance [3]. Designing future THz communication systems demands advances in micrometer-scale fabrication, thermal management, energy-efficient hardware, packaging, and the joint design of transceivers and MIMO antennas [4].

MIMO antenna systems employ several antennas at both the transmitting and receiving ends. The technology enables space-combining and diversity methods to send multiple signals over a channel. This may enhance channel capacity, data rate, spectral performance, coverage, and reliability, regardless of increasing bandwidth or power [5]. The efficacy of a MIMO antenna system depends largely on maintaining optimal radiation characteristics and minimizing mutual coupling among components. Consequently, the system requires substantial isolation, minimal envelope correlation, reduced reciprocal coupling, consistent radiation, and enhanced diversity [6]. MIMO

technology has been extensively implemented in fourth-generation long-term evolution and fifth-generation networks. It is expected to be employed in future sixth-generation communication systems [7]. These antennas are utilized in wireless local area networks, satellite communications, radar, Internet of Things, autonomous cars and other applications that need high capacity radio access [8].

The proposed quad-band Terahertz (THz) antenna is a promising applicant for many new monitoring and communication applications. The lower resonant bands of 2.61 and 3.5 THz and the impedance bandwidths of 0.6156 and 0.7822 THz can meet the needs of wireless communication over short distances with a high data rate and dense indoor 6G networks [9]. These frequency ranges can also be applied in combined communication and sensing applications, where the wide bandwidth and high frequency are helpful for both target recognition and simultaneous data relocation [10]. The THz imaging and spectroscopic applications are very interesting due to the more powerful resonant bands at 4.4531 and 6.25 THz with bandwidths of 0.815 and 1.5226 THz, respectively [11]. The broad bandwidth of the 6.25 THz resonance is also beneficial for high-resolution sensing, material characterization, and non-destructive testing [12]. Moreover, the multi-band response of the antenna enhances its flexibility for multifunctional systems, allowing it to operate at multiple THz frequency bands [13]. The broad impedance bandwidth, superior radiation, gain, efficiency, and isolation features of this functionally designed antenna make the device a viable candidate for upcoming high-data-rate THz communication, 6G wireless networks, integrated sensing and communication, THz optical imaging, spectroscopy, and advanced applications for sensing [14].

The recommended THz MIMO antenna technology integrated in future 6G communication scenarios is shown in Figure 1, which can enable resilient and rapid connections for a broad spectrum of smart applications [15]The recommended antenna demonstrates good electromagnetic performance, with broad impedance bandwidths of 0.6156 THz, 0.7822 THz, 0.815 THz, and 1.5226 THz, and multiband resonant operation at 2.61 THz, 3.5 THz, 4.4531 THz, and 6.25 THz. Moreover, the achieved high gain of 13.1076 dB, impressive isolation of −30.668 dB, a very low ECC of 0.012, a DG of 9.94 dB, and excellent radiation efficiency of 99.038% prove its ability to support high-capacity wireless communications with less interference and improved signal reliability. The exhibited THz MIMO aerial system can be a key enabling technology for new applications of 6G, such as smart city infrastructure, industrial IoT, UAV and aerial communication, satellite connectivity, smart transport, healthcare networks, and maritime surveillance [16]. The deployment of THz communication to UAV platforms can also provide further support for high-data-rate aerial communication, surveillance, sensing, and localization applications in future 6G networks [17]. In addition, because of the enormous accessible bandwidth and high spatial resolution, THz systems can be promising for advanced communication and sensing applications such as embedded sensing and communication (ISAC) in future networks such as 6G [18]. Moreover, the RLC equivalent circuit model effectively predicts the antenna properties, verifying the practical viability of the suggested design. The suggested THz MIMO antenna is a good contender for future smart wireless transmission systems due to its wideband operation, strong isolation, excellent diversity performance, and effective radiation performance [19].




Figure 1: THz MIMO antenna system conceptual framework for next 6G communication networks.

Table 1 evaluates the proposed terahertz MIMO antenna against prior designs, focusing on key parameters such as resonant frequency, impedance bandwidth, substrate material, board size, MIMO configuration, gain, isolation, coefficient of envelope correlation (ECC), diversity gain, radiation efficiency, and RLC equivalent-circuit modeling. Reference [20] describes a polyimide-based 4x4 MIMO antenna with resonance frequencies of 4.99 THz and 8.831 THz, bandwidth of 5.941 THz, gain of 11.89 dB, isolation of −27.34 dB, ECC of 0.001, diversity gain of 9.994 dB, and efficiency of 88.90%. Compared with the suggested antenna, this design has lower gain and efficiency, although it offers good isolation and ECC performance. Additionally, the suggested design achieves higher gain, better isolation, higher efficiency, and RLC analysis capabilities while using a small 1x2 MIMO setup. A polyimide-based antenna operating at 0.654 THz with a narrow bandwidth of 0.05 THz, gain of 11.67 dB, isolation of ≥25 dB, ECC of 0.003, diversity gain of 9.995 dB, and efficiency of 76.45% is reported in Reference [21]. Nevertheless, it is less efficient, has a smaller bandwidth, and lacks machine learning-based analysis when compared to the suggested antenna. Reference [22] describes a silicon dioxide-based 2x2 MIMO antenna operating at 7.5 THz with a bandwidth of 5.9 THz, gain of 8.3 dB, isolation of −16 dB, ECC of 0.005, and diversity gain of 9.97 dB. Compared with the suggested structure, this design has lower gain, lower isolation, higher ECC, and no RLC analysis, despite having an appropriate bandwidth. A polyimide-based 4x4 MIMO antenna operating at 0.395 THz and 0.629 THz with bandwidths of 0.01 THz and 0.025 THz, respectively, is described in Reference [23]. It has a gain of 5.17 dB, isolation of −20 dB, ECC of 0.0125, and efficiency of 92.48%. By contrast, the suggested antenna performs noticeably better than this design thanks to its multiple resonances, higher gain, broader bandwidth, improved isolation, lower ECC, and higher efficiency. A silicon dioxide-based antenna operating at 1.89 THz with a gain of 4.60 dB, isolation of −25 dB, incredibly low ECC of $15.6\times10^{-11}$, and efficiency of 74.5% is presented in the reference [24]. Its low gain, poor efficiency, and lack of RLC analysis limit its usefulness compared with the proposed architecture, despite its strong ECC performance. The polyimide-based 1x2 MIMO antenna described in Reference [25] operates at 0.35–0.75 THz with a bandwidth of 0.35–0.75 THz, achieves 82% efficiency, and provides −25 dB isolation. In contrast, the suggested antenna offers more advanced analytical capabilities, higher gain, greater isolation, higher efficiency, and a wider operational bandwidth. Reference [26] presents an FR-4-based antenna that performs at 0.86 THz with a bandwidth of 0.32 THz, gain of 4.04 dB, ECC of 0.0372, diversity gain of 9.99 dB, and efficiency of 70%. A polyimide-based antenna operating at 0.395 THz and 0.629 THz with bandwidths of 0.0095 THz and 0.024 THz, gains ranging from 3.89 to 5.17 dB, isolation of −20 dB, ECC of 0.0125, DG of 10 dB, and efficiency between 82% and 92.48% is described in the reference [27]. However, it has poor isolation, narrow bandwidth, lower gain, higher ECC, and no RLC integration. The suggested antenna offers much higher gain, lower ECC, improved isolation, better efficiency, and sophisticated RLC-based analysis compared to this design. A polyimide-based antenna with resonances at 0.445 THz and 0.540 THz, gain values between 6.6 and 7.9 dB, isolation of −20 dB, ECC values between 0.0001 and 0.10, and efficiency between 81.39% and 83.36% is presented in the reference [28]. The suggested antenna offers better electromagnetic performance, with higher gain, stronger isolation, higher efficiency, and additional RLC equivalent-circuit modeling analysis. With bandwidths of 0.6156, 0.7822, 0.815, and 1.5226 THz, respectively, the proposed polyimide-based 1×2 MIMO antenna operates at 2.61, 3.5, 4.4531, and 6.25 THz. It achieves a high gain of 13.1076 dB, strong isolation of −30.668 dB, ECC of 0.012, diversity gain of 9.94 dB, and an exceptional efficiency of 99.038%. The RLC equivalent-circuit model offers additional benefits for precise prediction and thorough performance evaluation. As a result, the proposed antenna performs well overall and is a strong applicant for future 6G wireless applications and THz MIMO communication. These qualities make it a strong potential for upcoming 6G terahertz communication, ultra-high-speed short-range communications, THz sensing, imaging, spectroscopy, biometric identification, material characterization, and security scanning applications.

Table 1: Performance evaluations of recommended and published works

| Ref | Resonance (THz) | BW (THz) | Substrate Materials | Board Size (λ) | MIMO Config | Gain (dB) | Isolation (dB) | ECC, DG (dB) | Efficiency (%) | RLC |
|---|---|---|---|---|---|---|---|---|---|---|
| [20] | 4.99, 8.831 | 5.941 | Polyimide | - | 4×4 | 11.89 | -27.34 | 0.001, 9.994 | 88.90 | No |
| [21] | 0.654 | 0.05 | Polyimide | 13.55λ× 24.84 λ₀ | - | 11.67 | ≥25 | 0.003, 9.995 | 76.45 | No |
| [22] | 7.5 | 5.9 | Silicon dioxide | 1.13 λ₀× 1.13 λ₀ | 2×2 | 8.3 | -16 | 0.005, 9.97 | - | No |
| [23] | 0.395, 0.629 | 0.01, 0.025 | Polyimide | 6.45 λ₀× 7.74 λ₀ | 4×4 | 5.17 | -20 | 0.0125, 10 | 92.48 | No |
| [24] | 1.89 | (1.41-3.0)1.59 | Silicon dioxide | 0.35 λ₀× 0.23 λ₀ | - | 4.60 | -25 | $15.6\times10^{-10}$, ≈ 10 | 74.5 | No |
| [25] | - | (0.35-0.75)0.4 | Polyimide | 5.47 λ₀× 2.73 λ₀ | 1×2 | - | -25 | - | 82 | No |
| [26] | 0.86 | 0.32 | FR-4 | 2.73 λ₀× 2.73 λ₀ | - | 4.04 | - | 0.0372, 9.99 | 70 | No |
| [27] | 0.395, 0.629 | 0.0095, 0.024 | Polyimide | 9.11 λ₀× 10.94 λ₀ | 4 | 3.89, 5.17 | -20 | 0.0125, 10 | 82, 92.48 | No |
| [28] | 0.445, 0.540 | - | Polyimide | 28.11λ₀ × 18.06 λ₀ | 4 | 7.9, 6.6 | -20 | 0.0001, 10 | 81.39, 83.36 | No |
| Proposed | 2.61, 3.5, 4.4531, 6.25 | 0.6156, 0.7822, 0.815, 1.5226 | Polyimide | 1.827λ₀ × 0.783 λ₀ | 1×2 | 13.1076 | -30.668 | 0.012, 9.94 | 99.038 | Yes |

The recommended polyimide-based 1 × 2 THz MIMO antenna may work in four bands at 2.61, 3.50, 4.4531, and 6.25 THz, with impedance bandwidths of 0.6156, 0.7822, 0.815, and 1.5226 THz. It occupies a tiny normalized area of 1.827λ₀ × 0.783λ₀ and achieves a highest gain of 13.1076 dB. The inter-element isolation of -30.668 dB confirms the efficient decrease of mutual coupling. An envelope correlation coefficient of 0.012 and a diversity gain of 9.94 dB indicate low correlation and excellent diversity performance. The antenna has good electromagnetic radiation for all bands, with a radiation efficiency of 99.038%. The resonant properties can also be described at the circuit level using the RLC equivalent circuit model. The results indicate that the antenna is a compact high-performance candidate for multiband THz communication, sensing, imaging, and future 6G wireless applications [29].

**Research Gap and Contribution:**

Although THz (terahertz) antennas and MIMO configurations for future 6G communication systems have been widely studied, several challenges remain unsolved. Modern THz MIMO antennas often involve trade-offs between compactness and electromagnetic performance, particularly in impedance bandwidth, gain, radiation efficiency, isolation, and mutual coupling. The previous works identified in this study either used 2×2 or 4×4 MIMO antenna arrays or showed limited performance in bandwidth, diversity gain, isolation, or size. For example, THz MIMO antennas reported in the literature are typically realized on polyimide and silicon dioxide substrates with thin-film electronics, resulting in only moderate bandwidth, efficiency, and gain. Most prior work lacks an equivalent RLC circuit model needed to provide a fundamental electromagnetic circuit-theory basis for full-wave analysis of a resonant THz MIMO system. Therefore, it is necessary to develop an affordable, reliable THz MIMO antenna with multiband operation and good impedance matching, unity gain, radiation efficiency, low mutual coupling, ECC, and diversity.

- The first contribution concerns the design and development of a tiny 1×2 THz MIMO antenna on a flexible polyimide substrate. The proposed structure achieves a miniature size of 1.827λ₀ × 0.783λ₀ and provides four resonant frequencies at 2.61, 3.50, 4.4531, and 6.25 THz, along with broad impedance bandwidths.

- The second modification involves selecting a graphene-based radiating patch and a flexible polyimide substrate. We obtained the modified radiator through a series of geometric enhancements to improve impedance matching, current distribution, gain, and radiation characteristics in the desired THz frequency range.
- A third contribution of this paper is that the antenna achieves multiband operation with high gain and radiation efficiency. In this study, we design four operating bands; the peak gain reaches 13.1076 dB, and the radiation efficiency reaches 99.038%, which is highly significant for THz applications.
- The fourth contribution is enhancing MIMO isolation and diversity performance without adding any decoupling structure. The orthogonal feeding arrangement reduces mutual coupling, and isolation exceeds −30.668 dB, with a very low ECC of 0.012 and a diversity gain of about 9.94 dB.
- The fifth contribution is the systematic optimization of the characteristics and shape of the antenna. We optimize key parameters, such as substrate thickness, feed width, and ground-plane thickness, for superior performance, including impedance matching, gain, and radiation efficiency at the THz frequencies under investigation.
- The sixth contribution is to construct an RLC comparable circuit model and validate it against the CST simulation findings. The close agreement between the CST and ADS results suggests that the proposed circuit model may replicate the antenna's resonant and impedance properties.

**The Characteristics of Graphene Materials:**

Graphene is a common material used in ultra-fast, high-frequency communication systems. Graphene is an individual layer of carbon atoms arranged in a honeycomb configuration [30]. Graphene is a highly suitable material for high-frequency, extremely wide-band THz antennas in the 0.1–10 THz frequency range because it is structurally versatile, has great electron mobility, and excellent electrical conductivity [31]. Graphene enables surface plasmon polaritons (SPPs) at THz frequencies and so opens the possibility for the manufacture of very small, low-loss, and high-efficiency antennas [32]. The conductivity is capable of being precisely regulated by changing the corresponding chemical potential (usually 0.1–0.5 eV) via electrostatic or doping with chemicals [33]. This permits frequency tweaking and lowers energy loss with a corresponding relaxation time of 1 ps and ultra-thin thickness (0.01 μm in models). Conventional simulation parameters are T = 300 K, μc = 0.5 eV, τ = 1 ps, thickness = 0.01–500 μm, and a frequency sweep from 0.1 to 10 THz with 1000 points. The structural flexibility and near transparency of graphene make it suitable for wearable devices, versatile, and confined space applications [34]. But the large-scale assembly and the circuit integration process are still tough, and hurdles need to be faced to be able to take full advantage of the potential of graphene for 6G, high-speed data transmission at high speeds, and modern sensing technology applications [35].

**Design Methodology:**

The systematic design evolution approach given in Figure 2 is employed to design the recommended THz MIMO antenna system for future super-fast, smart, intelligent THz communication systems. The recommended antenna is developed stepwise to evolve from a single radiator baseline towards a 1x2 MIMO configuration. The radiating patch is made of graphene, which provides strong field confinement mechanical flexibility, tuneable chemical potential through electrostatic gating and superior electrical conductivity, thus high radiation efficiency, broad impedance bandwidth and best matching of impedance are obtained. The flexible polyimide substrate with low dielectric loss provides mechanical endurance and strong compatibility with flexible electronic devices, while achieving very low signal propagation losses. The base plane consists of annealed copper, which offers an extremely conductive and mechanically stable current return path, avoiding the occurrence of spurious surface-wave excitations and increasing the overall efficiency. The architecture extends the single radiator to a 1x2 anti-parallel MIMO system. Pattern and spatial diversity greatly increase spectral efficiency while reducing mutual coupling. The parameters for antenna design are presented in the section of Table 2. Graphene's surface conductivity can be electrostatically varied dynamically; therefore, the architecture offers real-time frequency reconfigurability. The antenna patch is made of graphene, and the ground plane is copper with a thickness of 0.2 μm for optimal performance and minimal size. The complex design elements, such as a solid ground plane, feedline insets, 6-segment cylindrical shape, L-shape, and line shapes, were designed with CST Studio Suite to increase gain and bandwidth and improve reflection-coefficient performance. The MIMO antenna has an overall dimension of 210 × 90 $\mu m^2$. CST simulations show that the return loss, radiation pattern, and gain are highly efficient. It is a lightweight, adaptable, and highly productive solution for next-generation cellular communication systems.

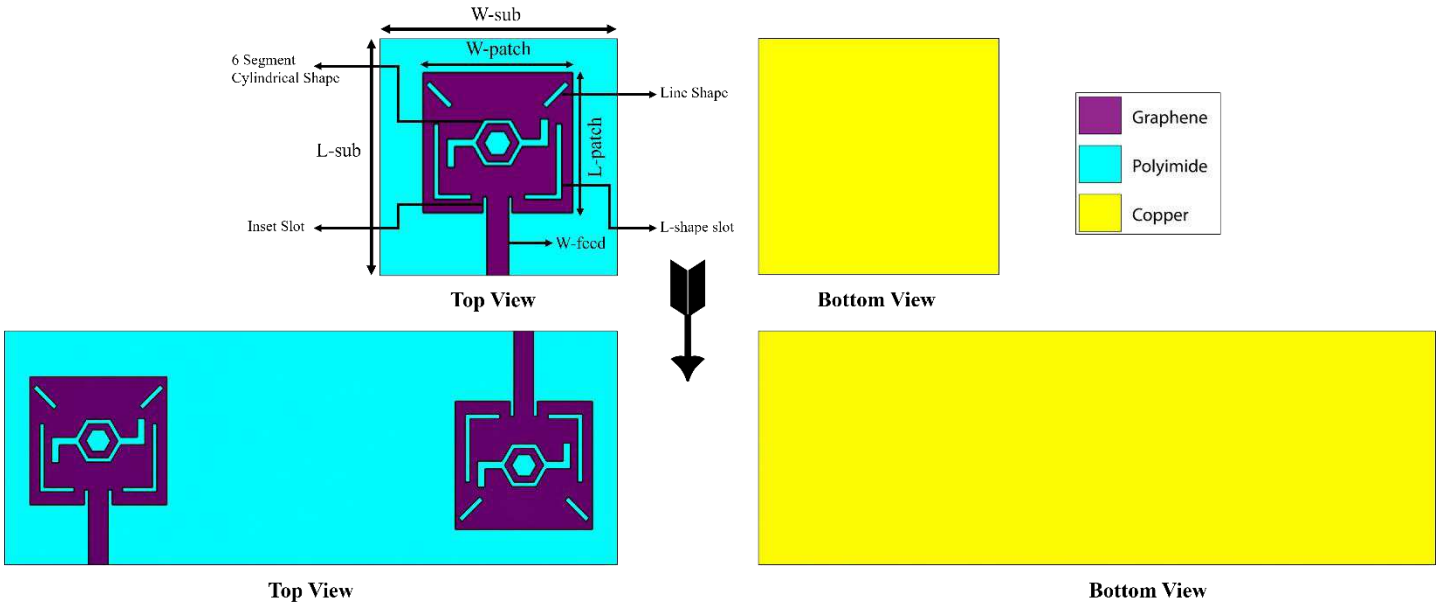



Figure 2: Evolutionary mechanism from a one-element antenna to a MIMO Antenna.

Table 2: Antenna Drawing Variables

| Drawing Variables | Indication | Measure (µm) | Drawing Variables | Indication | Measure (µm) |
|---|---|---|---|---|---|
| Substrate Width | W-sub | 90 | Substrate Thickness | h-sub | 25 |
| Substrate Length | L-sub | 90 | Ground Thickness | t-gnd | 0.2 |
| Patch Width | W-patch | 56 | Patch Thickness | PT | 0.01 |
| Patch Length | L-patch | 52 | Distance Between Two Antennas | DW | 30 |
| Feed Width | W-feed | 8 | | | |

**Single-Element Antenna:**

We developed a new single-element antenna that is more efficient and superior to the current one. We determined the antenna dimensions and materials through simple mathematical calculations, and improved its performance and operation through proper engineering. These approaches have achieved precision in the patch dimensions:

Effective Dielectric Constant ($\epsilon_{eff}$): $$\epsilon_{eff} = \frac{\epsilon_r+1}{2} + \frac{\epsilon_r-1}{2}\left(1+12\frac{h}{w}\right)^{-\frac{1}{2}} \quad (1)$$

Patch Width (W): $$W = \frac{c}{2f}\sqrt{\frac{2}{\epsilon_r+1}} \quad (2)$$

Patch Length (L): $$P\,L = \frac{c}{2f\sqrt{\epsilon_{eff}}} - 2\Delta L \quad (3)$$

Extension Length (ΔL): $$\Delta L = 0.412h\frac{(\epsilon_{eff}+0.3)\left(\frac{W}{h}+0.264\right)}{(\epsilon_{eff}-0.258)\left(\frac{W}{h}+0.8\right)} \quad (4)$$

Here,

i. λ is the wavelength, the gap over which the structure of the electromagnetic spectrum repeats itself.
ii. c is the speed of light, about $3\times10^8$ m/sec.
iii. $\epsilon_r$ is the dielectric constant of the substrate material (3.5 for polyimide).
iv. f is the operational frequency.
v. $\epsilon_{eff}$ is the effective dielectric constant, considering the impact of the wave propagation on the substrate.

These mathematical statements form the basis for antenna structure design, accuracy, and efficiency in THz applications.

Figure 3 demonstrates the structure and materials of the one-element antenna designed for the 6G terahertz (THz) wireless networking infrastructure. As shown, the entire structure is miniaturized and built at the micrometer (μm) scale to meet the high-frequency requirement. The flexible polyimide substrate offers excellent mechanical properties, low dielectric loss, and good thermal stability, making it a promising candidate for modern flexible electronic devices. The top view shows that the radiating patch is made of high-conductivity graphene and features designed geometric shapes and a microstrip feed line. The designed geometry improves impedance matching, current distribution, and ultra-wideband performance. In particular, it achieves an extraordinary resonant frequency in the terahertz range. The bottom view shows that the bottom layer is a full copper ground plane, which provides a better reflecting surface for the electromagnetic field. Overall, the design significantly improves power-transfer capability. In addition, eliminating back-lobe radiation can improve radiation efficiency. Using a highly conductive graphene patch and a micrometer-scale PI substrate, the single-element graphene antenna achieves enhanced performance for ultra-high-frequency information transmission; thus, it is promising for terahertz sensing and 6G terminal equipment.

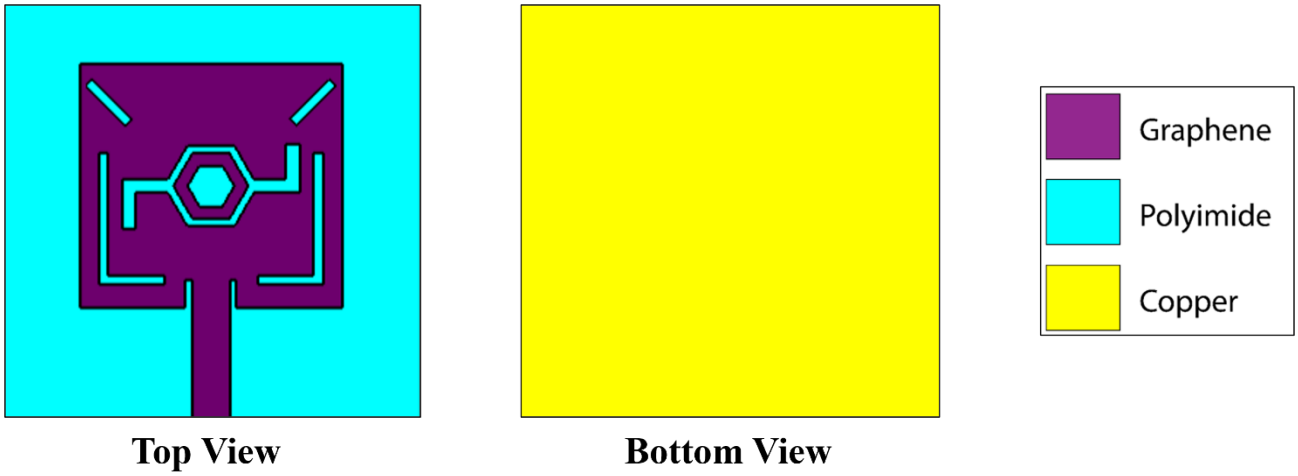



Figure 3: Top and bottom views of a single-element THz antenna.

**Single Element Evaluation:**

This research proposes an optimized single-element antenna design to improve electromagnetic performance in the terahertz frequency band. It consists of a graphene-based radiating patch on a dielectric substrate and a continuous copper ground plane on the reverse side to ensure stable radiation behavior and minimize back radiation. We developed the radiating component in three stages to improve radiation characteristics, current distribution, and impedance matching. The first baseline arrangement is a typical rectangular patch. Next, we integrate a hexagonal resonator into the patch to improve impedance characteristics and effective current flow. Further slot loading and edge tweaks increase surface current, electromagnetic coupling, and radiation efficiency. Figure 4 This illustration shows how the antenna evolved with each iteration, allowing us to see incremental improvements over time. The effects of these associated corresponding geometrical adjustments are investigated by assessing the reflection coefficient, gain, and efficiency of radiation in the frequency range of 1.5-6.5 THz. The improved arrangement is more suitable for high-frequency THz sensing and communication, with better impedance matching, gain, and radiation performance.

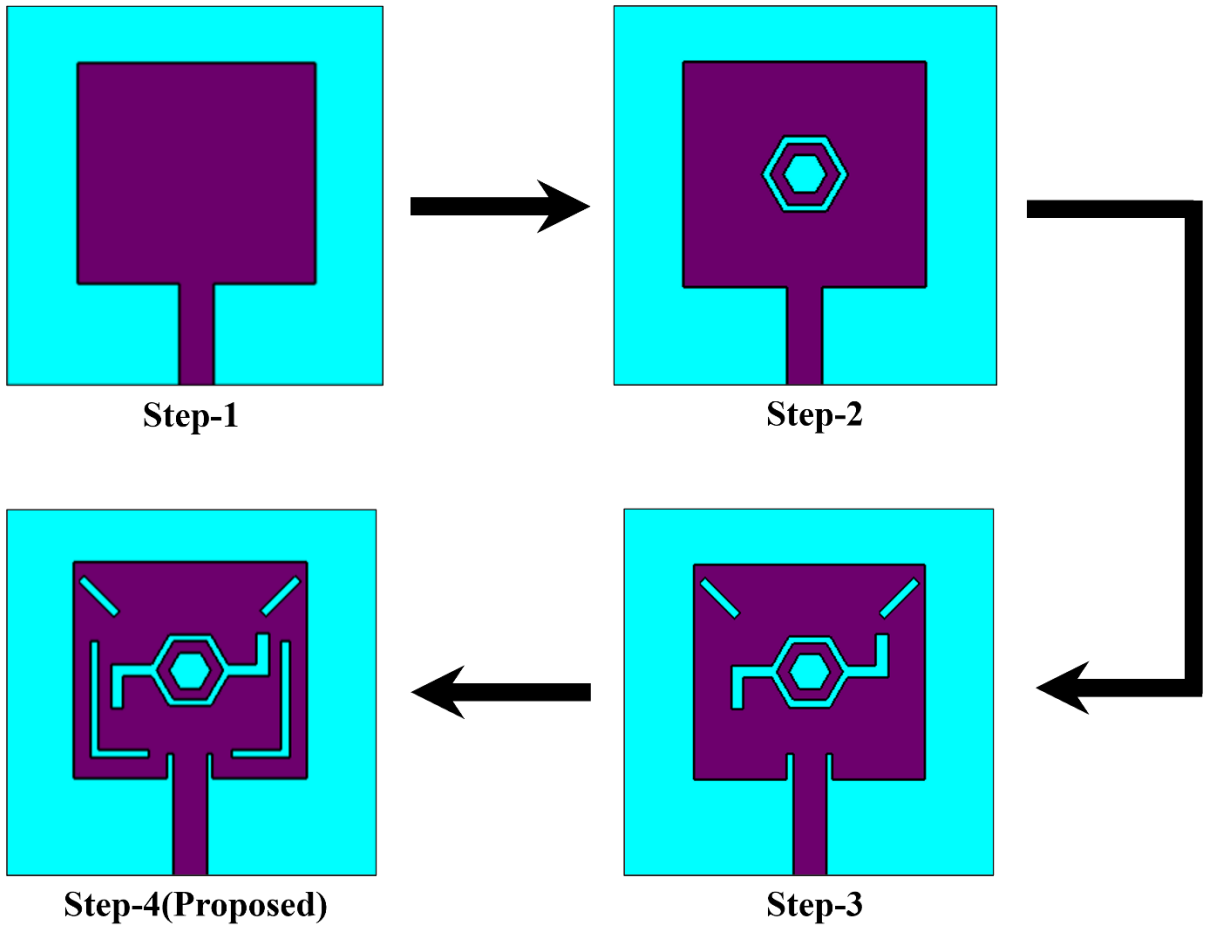



Figure 4: An Overview of the Single-Element Antenna Design.

The proposed single element of the THz antenna is depicted in Figure 5 in the frequency range of 1.5-6.5 THz. We evaluated the antenna's radiation efficiency, gain, and reflection coefficient (S11) at four design stages. The numerical comparison clearly shows that incorporating and optimizing the extra geometric factors led to progressive improvement.

Step 1 (Baseline Design): The baseline design shows relatively weak, scattered resonant responses in the frequency range under study. The baseline design has several shallow resonances and the deepest S11 resonance of −29 dB at 3.3 THz, as illustrated in Figure 5(a). The gain is illustrated in Figure 5(c), and is 0 dB at 1.5 THz and gradually increases up to 10.8 dB at 6.5 THz toward the upper frequency region. The associated radiation efficiency is shown in Figure 5(b) is in the range of 77–90%, with the minimum efficiency in the 2.7–3.0 THz range. Thus, the basic framework possesses the fundamental radiation properties, but its impedance matching is limited, and its efficiency in the operating band is relatively unstable.

Step 2 (First revision): The hexagonal resonator significantly improved the electromagnetic response of the structure compared to the resonator structure of Figure 5. Figure 5(a) demonstrates the enhanced resonance depth at –32 dB at 3.1 THz for the fundamental configuration, while Figure 5(a) shows the S11 response. For the frequency range of interest in Figure 5(c), the gain rises steadily from 0.5 dB at 1.5 THz to 10.2 dB at 6.5 THz. At the same time, the radiation efficiency was relatively high at 80-92%, peaking at 92% at 1.5 THz. The improved S11 response as well as the high efficiency observed by introducing the hexagonal resonator can be explained by a better electromagnetic coupling related to an improved distribution of current.

Step 3 (further refinement): The geometry was further refined to enhance further the performance of the antenna. The S11 parameter data is shown in Figure 5(a), where the dominant resonance peaks at −29 dB at 3.5 THz, with other resonances occurring at different frequencies, as expected. Also, the matching gain is improved and reaches the peak of 10.9 dB at 6.5 THz as shown in Figure 5(c). Also, the radiation efficiency was improved up to a maximum of 90% at 6.5 THz, varying from 79 to 90% at Figure 5(b). This modification resulted in more resonances, better radiation performance and more uniform current distributions.

Step 4 (final design suggested): The fourth step is the best one among all steps, which is the end of evolution. The presented monopole antenna in Figure 5(a) depicts a considerably deep S11 resonance of -46 dB at 3.1 THz due to good matching of impedance, and a significant reduction of the reflected power, while several resonances can be observed over the whole frequency range. The gain is

substantially higher than in the preceding phases, as shown in Figure 5(c), with a maximum of 11.828 dB at 5.75 THz. The gain coefficient remains above 10 dB from 5.5 THz to 6.5 THz, indicating robust performance at higher frequencies. Figure 5(b) shows that the radiation efficiency can reach 97.5% at 1.5 THz. It is generally above 80% across the examined frequency range. Therefore, the final design shows much better impedance matching, radiation gain, and radiation efficiency than the preceding designs. Step 4, The final optimized recommended setup is depicted. The evolution indicates that repetitive geometrical adjustments can considerably improve the antenna's wireless performance.

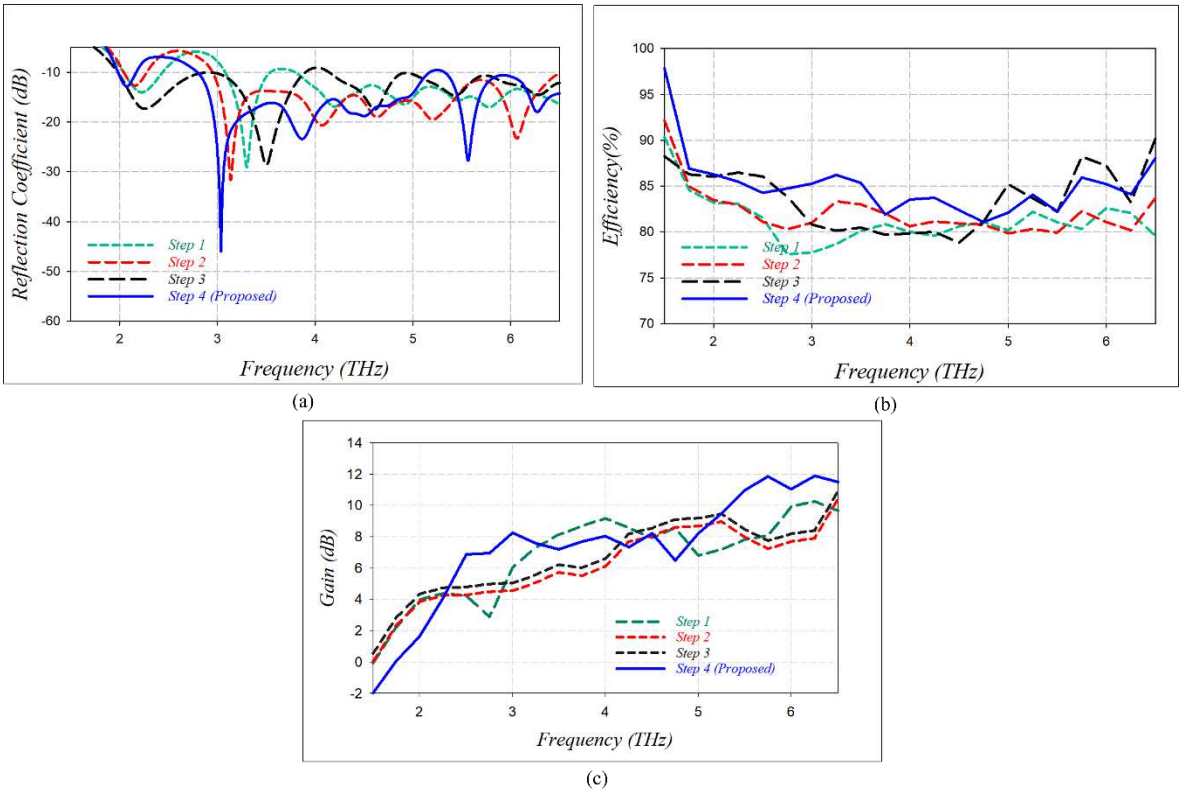



Figure 5: Evolutionary Development of the Single Element Antenna Architecture (a) Reflection Coefficient (b) Efficiency (c) Gain.

**Parameter Analysis:**

Some basic parameters are employed to optimize the structure of a single-element patch antenna for THz applications [36]. The antenna's radiation parameters and operating frequency range are important in choosing the substrate quality and patch size. Substrate quality and patch size also affect the antenna's radiation characteristics and operating frequency range. The influence of the feed width, substrate height, and ground thickness on the effectiveness of the antenna is addressed in this paper [37]. The antenna's impedance bandwidth, the surface wave propagation, and the radiation efficiency are strongly dependent on the substrate height. Moreover, the current distribution and overall electromagnetic activity of the antenna are also determined by the material thickness of the ground sphere. In order to enhance the power supply as well as the return loss (S11), the feed width is adjusted to achieve an adequate impedance matching between the feed mechanism and the patch [38]. The polyimide substrate is used as a dielectric material due to its low losses and acceptable dielectric properties at the THz frequencies [39]. Thus, the design is suitable for high-end THz cellular communication, detecting, and surveillance since such parameters can be tuned to improve the antenna performance, e.g., radiating efficiency, bandwidth, gain, and matching of impedance [40].

**Substrate Thickness Analysis:**

Figure 6 displays the dependence of the recommended THz antenna performance on the substrate thickness (h-sub), in the frequency range of 1.5-6.5 THz, expressed as radiating efficiency, gain, and reflection coefficient (S11). The results are presented for three substrate thicknesses: h-sub = 30 µm (green dotted line), h-sub = 20 µm (red dashed line), and h-sub = 25 µm (blue solid line, proposed design). The impedance matching is best for h-sub = 25 µm, as shown by the reflection coefficient (S11) in Figure 6(a). In this case, the resonance spots are more well-defined than for the other substrate thicknesses. Specifically, the 3.0 THz structure has the lowest possible S11 of −45 dB. This indicates excellent impedance matching and efficient excitation of the antenna mode. In contrast, for the h-sub=20 and h-sub=30 structures, the reflection coefficients are higher, indicating worse impedance matching in these two cases. A similar situation appears in Figure 6(c): radiation, expressed as gain, is best for the h-sub = 25 µm antenna among the cases considered. At 6.25 THz, the

maximum gain exceeds 11.8777 dB [see Figure 6(c), the dependence of gain on frequency]. For the other antenna configurations, the gain values are lower because the non-ideal substrate thickness alters the radiation characteristics and the electromagnetic field distribution. A similar trend is observed in Figure 6(b), which shows the variation in radiating efficiency. The values decrease for thin and thick substrates, while the h-sub = 25 µm design provides higher efficiency across the entire operating band. Therefore, the appropriate substrate thickness for the suggested THz antenna is h-sub = 25 µm, which provides acceptable radiating efficiency, gain, and impedance matching.

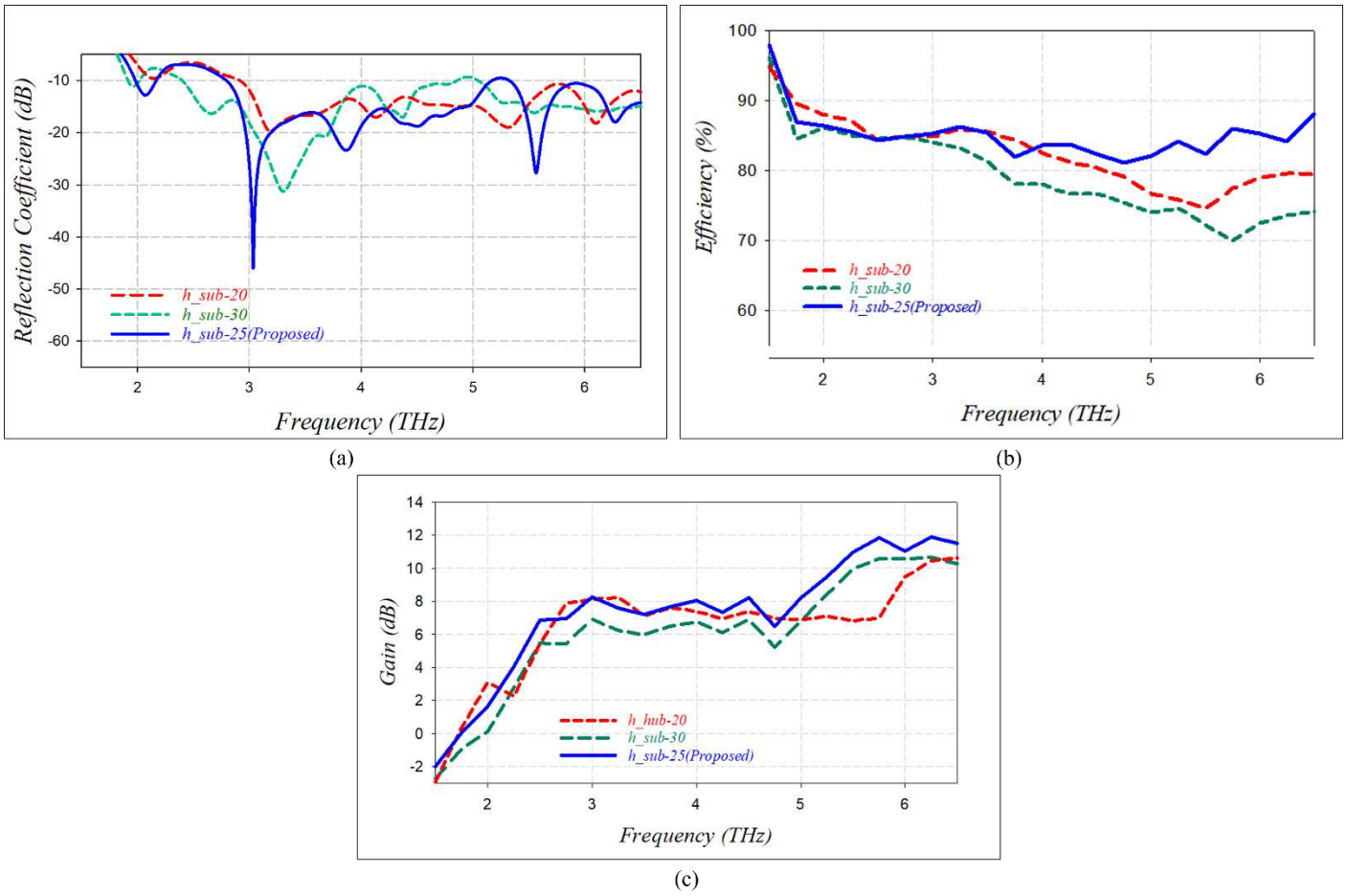



Figure 6: Performance effects of Substrate thickness variations: (a) Reflecting coefficient, (b) Efficiency, (c) Gain.

**Feed Width Analysis:**

The efficiency of the proposed THz antenna is shown in Figure 7 in a frequency range of 1.5–6.5 THz. The effect of changes in the feed width (W-feed). Three feed widths are examined: W-feed = 8 µm (blue solid line; recommended design), W-feed = 16 µm (green dashed line), and W-feed = 4 µm (red dashed line). We characterize their performance by radiating efficiency, gain, and impedance matching. The W-feed = 8 µm design shows the best impedance matching performance of all the designs from the coefficient of reflection (S11) response, as shown in Figure 7(a). It resonates deeply at 3.0 THz with S11 equal to −45 dB, implying a good power transfer between the radiating element and feeding structure. However, the W-feed = 4 µm and W-feed = 16 µm configurations show poor matching because more reflection occurs in different resonance regions. The gain characteristics are shown in Figure 7(c), where the W-feed = 8 µm design maintains high gain across the entire frequency range, with a maximum gain of 11.8777 dB at 6.25 THz. The other feed widths show less gain across the band. Moreover, the radiation efficiency comparison in Figure 7(b), shows the better performance of W-feed = 8 µm, which is above 80% over the band and reaches 97.8449% at lower frequencies. For the proposed THz antenna design, we choose W-feed = 8 µm as the best feed width, yielding better impedance matching, higher gain, and higher radiation efficiency.

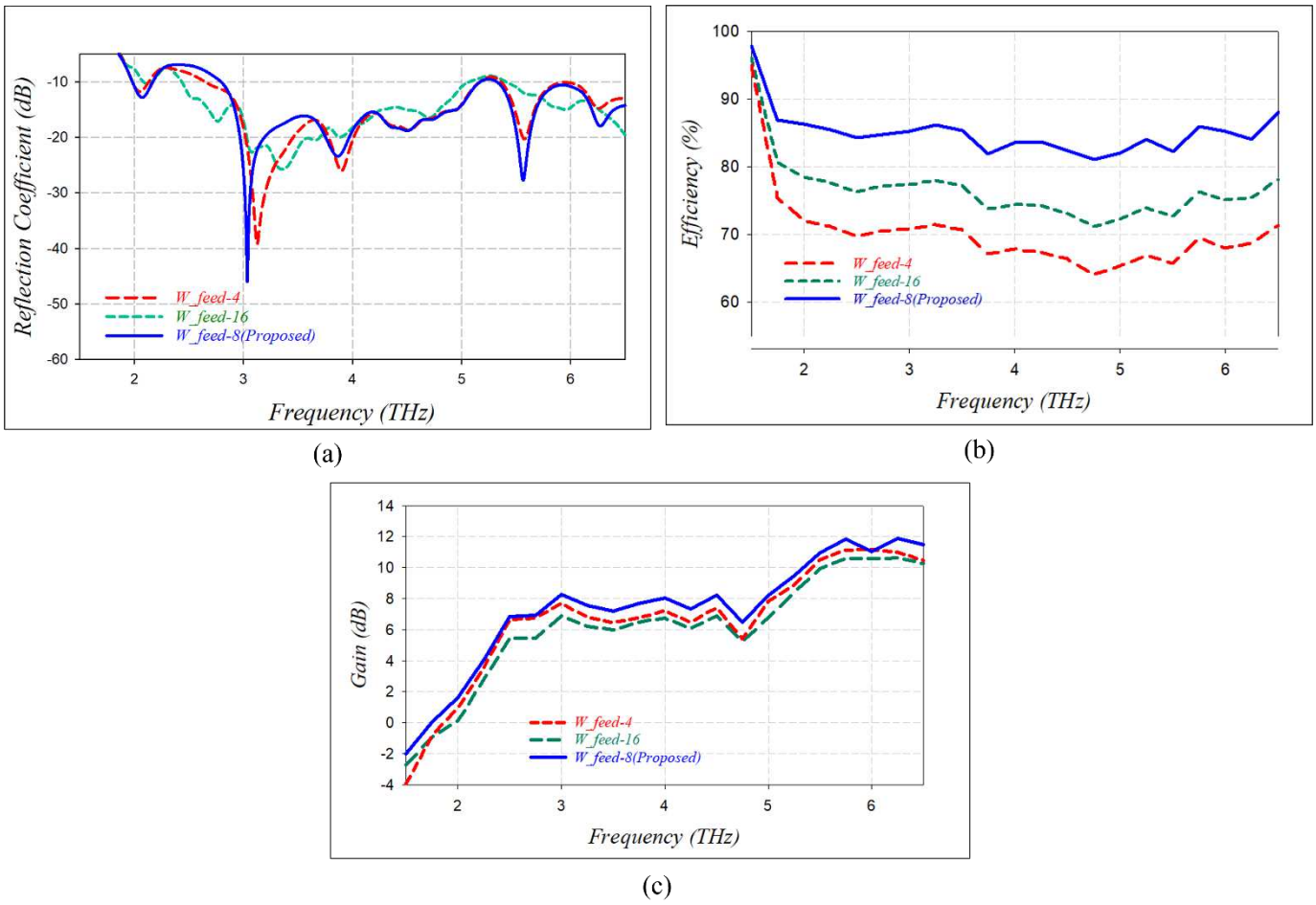



Figure 7: Influence of Adjusting Feed Width on Antenna Metrics: (a) Reflection Coefficient; (b) Efficiency; (c) Gain.

**Ground Thickness Analysis:**

The effect of the thickness of the ground (t-gnd) on the proposed THz antenna working in the frequency range of 1.5–6.5 THz is presented in Figure 8. We consider three ground-thickness cases: t-gnd = 0.1 μm (red dashed line), t-gnd = 0.2 μm (blue solid line, the suggested design), and t-gnd = 0.6 μm (green dashed line). They are evaluated in terms of radiating efficiency, gain, and the reflection coefficient (S11). The coefficient of reflection is presented in Figure 8(a). It is observed that for t-gnd = 0.2 μm there is the best matching of the impedance among the considered cases. This is illustrated by the lowest reflection coefficient at 3.05 THz, equal to −45 dB. For the same case, the second resonant frequency is observed at 5.35 THz. The cases t-gnd = 0.1 μm and t-gnd = 0.6 μm show poorer input-impedance matching and therefore higher S11 values in the operating frequency band. The maximum gain is observed in Figure 8(c) for the case of t-gnd = 0.2 μm, equal to 11.8777 dB at 6.25 THz. As expected, the other cases have lower gain at higher frequencies. In Figure 8(b), the radiating efficiency for all three cases is presented. Again, the best performance is shown for t-gnd = 0.2 μm. At lower frequencies, the radiating efficiency is 97.8449%, while across the rest of the frequency band, it remains above 80%. Consequently, the optimal ground thickness is t-gnd = 0.2 μm for the proposed THz antenna. This provides the best balance between radiating efficiency, gain, and input impedance matching.

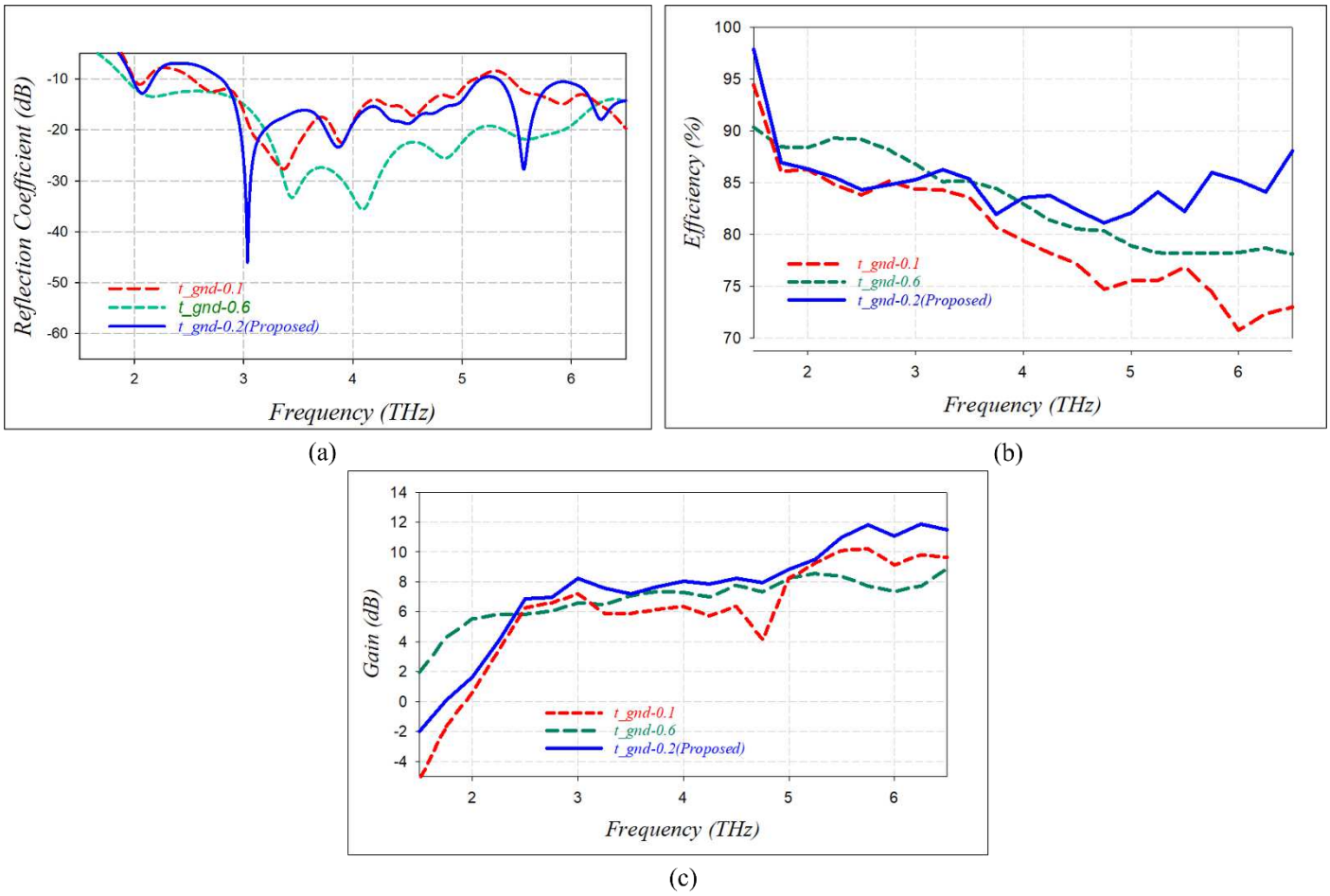



Figure 8: Influence of Variation in Ground Thickness on Antenna Performance: (a) Reflection Coefficient; (b) Efficiency; (c) Gain.

**MIMO Antenna Analysis:**

Modern wireless communication has improved network performance, reliability, and data transfer rates through Multiple-Input Multiple-Output (MIMO) antenna technology. This approach uses multiple input/output antenna elements to broadcast multiple data streams concurrently, maximizing channel throughput and spectrum efficiency. This approach reduces the effects of multipath fading and interference; through spatial diversity and multiplexing, it improves link quality. MIMO antennas are key components in developing sixth-generation (6G) wireless networks because they can improve coverage and throughput. MIMO beamforming is also employed in wireless communication to improve network signal quality and reduce interference. Hence, MIMO is critical to enabling the Internet of Things (IoT) and smart infrastructure, and it boosts the performance of sixth-generation wireless networks. IoT and mobile communication rely on MIMO to meet the demand for higher data rates, as modern mobile networks need them to stay connected. To maximize channel throughput and spectrum efficiency, wireless communication networks rely on MIMO. Businesses and consumers increasingly rely on technology that requires higher data rates to operate. Therefore, MIMO antennas can improve wireless connectivity. In Figure 9We compared the three MIMO topologies in terms of radiation efficiency, isolation, and spatial diversity to evaluate different spatial orientations and feeding processes. Two square patch radiators with the slot-type etching implemented in the radiating elements were integrated to form Antenna 1, as seen in Figure 9(a). The microstrip feed line is placed on the horizontal axis, and accordingly, it is at the farthest left and right positions on the substrate to execute the feeding mechanism, as shown in the figure. Similarly, Figure 9(b) shows how antenna 2 was modified to achieve parallel polarization and symmetrical current distribution by shifting the feeding point at the bottom of each radiator in a vertical design. Additionally, the modification of the final suggested antenna is seen in Figure 9(c) with one radiator patch rotated to place the two feed lines on opposite sides (top and bottom). This arrangement gives the two ports mutually orthogonal spatial orientation, eliminating the need for further decoupling elements. Each replication has the same ground-plane impedance-matcher arrangement projected on its right side. By modifying the feeding location, radiator patch rotation, and surface-current routing, isolation, bandwidth, and radiation efficiency can be varied. These features are the essential factors affecting the MIMO antenna performance in 6G wireless communications and high-frequency applications.

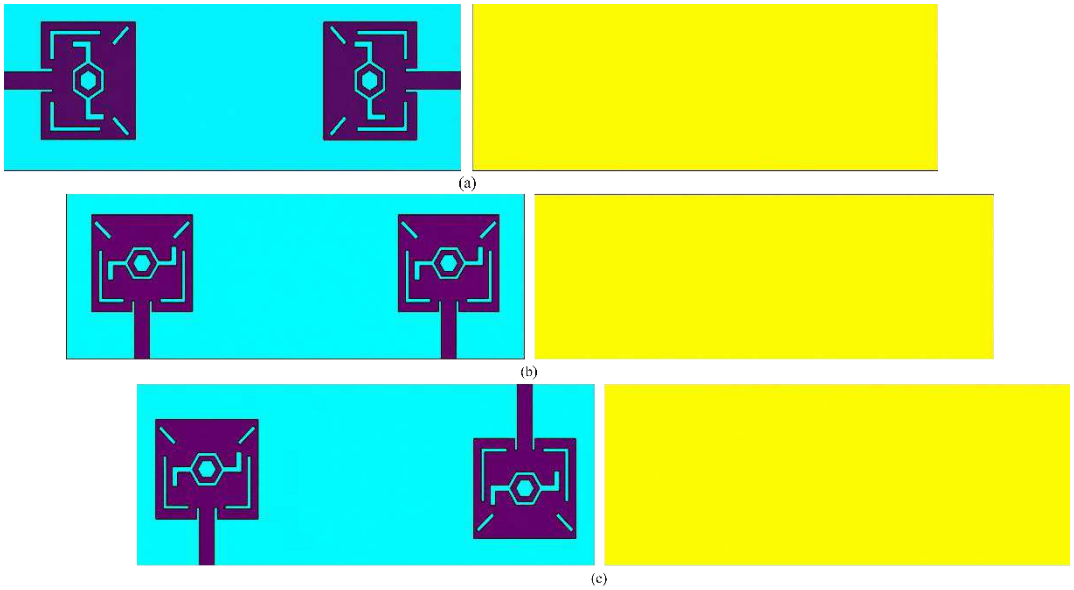



Figure 9: Assessment of MIMO Antenna Configurations:(a) Antenna-1; (b) Antenna-2;(c) Proposed Antenna.

**MIMO Antenna Result:**

The comparative results of the assessed antenna topologies is shown in Figure 10 which amply illustrates the suggested design's advantage over reference structures. Antenna 1 has an operational bandwidth of 2.97–5.05 THz, the edge gain of 10.2 dB, a lowest isolation of -54.017 dB, a resonance peak of -25.7288 dB at 3.355 THz, and an efficiency of 96.3%. By contrast, Antenna 2 has the lowest isolation (-39.259 dB), a resonance peak of -25.366 dB at 2.579 THz, fragmented bandwidth segments, a top gain of 11.1 dB, and an efficiency of 95.7%. The proposed antenna, from opposite aspect, achieves an exceptionally deep resonance peak of -53.71 dB at 2.61 THz, continuous wide bandwidths across four major bands (0.6156, 0.7822, 0.815, and 1.5226 THz), the edge realized gain of 13.1076 dB within the functioning bandwidth, unique port isolation (S21) below -30.668 dB (reaching a minimum isolation (S21) of -67.4517dB), and an exceptional radiation efficiency of 99.038%. Overall, we chose the proposed antenna for its superior gain and efficiency, improved isolation, wider bandwidth coverage, and excellent impedance matching.

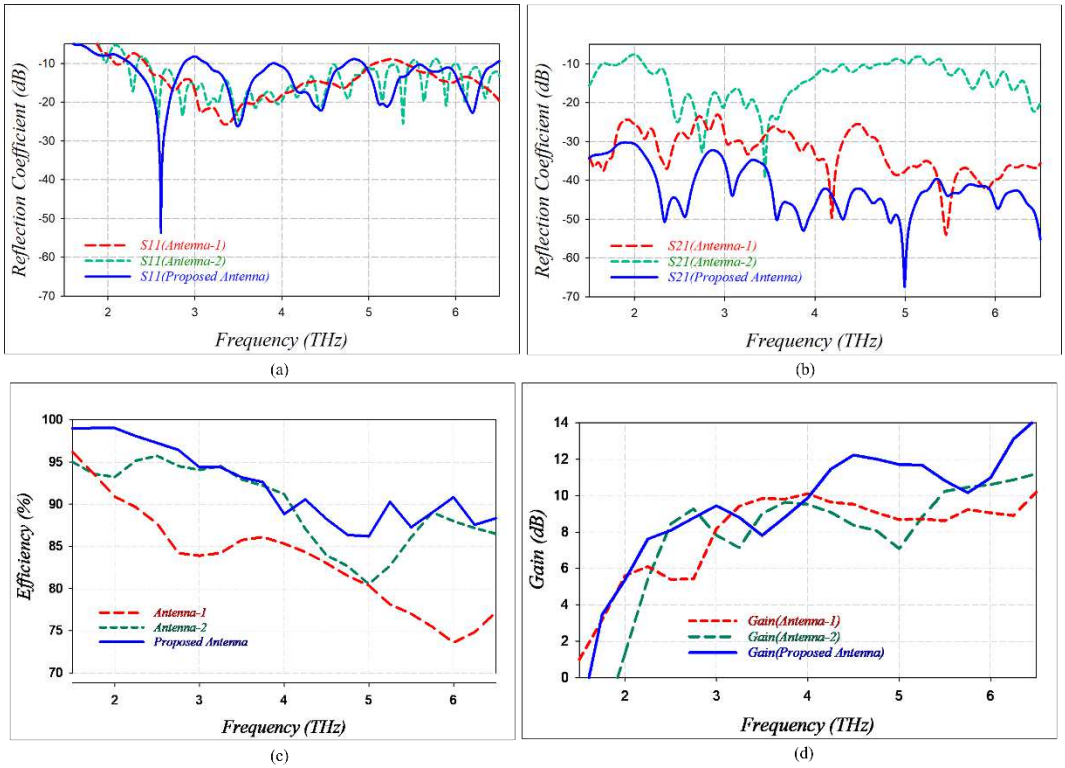



Figure 10: Analysis of the Performance Metrics for Three MIMO Antenna Configurations:(a) S11; (b) S21; (c) Efficiency; (d) Gain.

**Analysis of Single-Element Antenna vs MIMO Antenna:**

Figure 11 This figure compares the designed MIMO antenna with a single-element antenna, assessing radiating efficiency, gain, and the reflection coefficient over the 1.5–6.5 THz range. The MIMO antenna keeps the coefficient of reflection below -10 dB across most of the spectrum and shows more stable resonance with multiple deep resonance spots, indicating better impedance matching. It also has a wider gain range of 7.8572 dB to 11.8777 dB from 2.5 THz to 6.5 THz, compared to 7-13 dB for the single-element antenna. The single-element antenna's radiation efficiency ranges from 81.0827% to 88.0629%, while the MIMO antenna's radiation efficiency remains above 85% across the band and reaches 99% at the lowest frequencies. The results confirm that the proposed MIMO antenna exhibits impedance matching, sensitivity gain, and high radiated efficiency, which are well suited to efficient THz cellular communication scenarios.

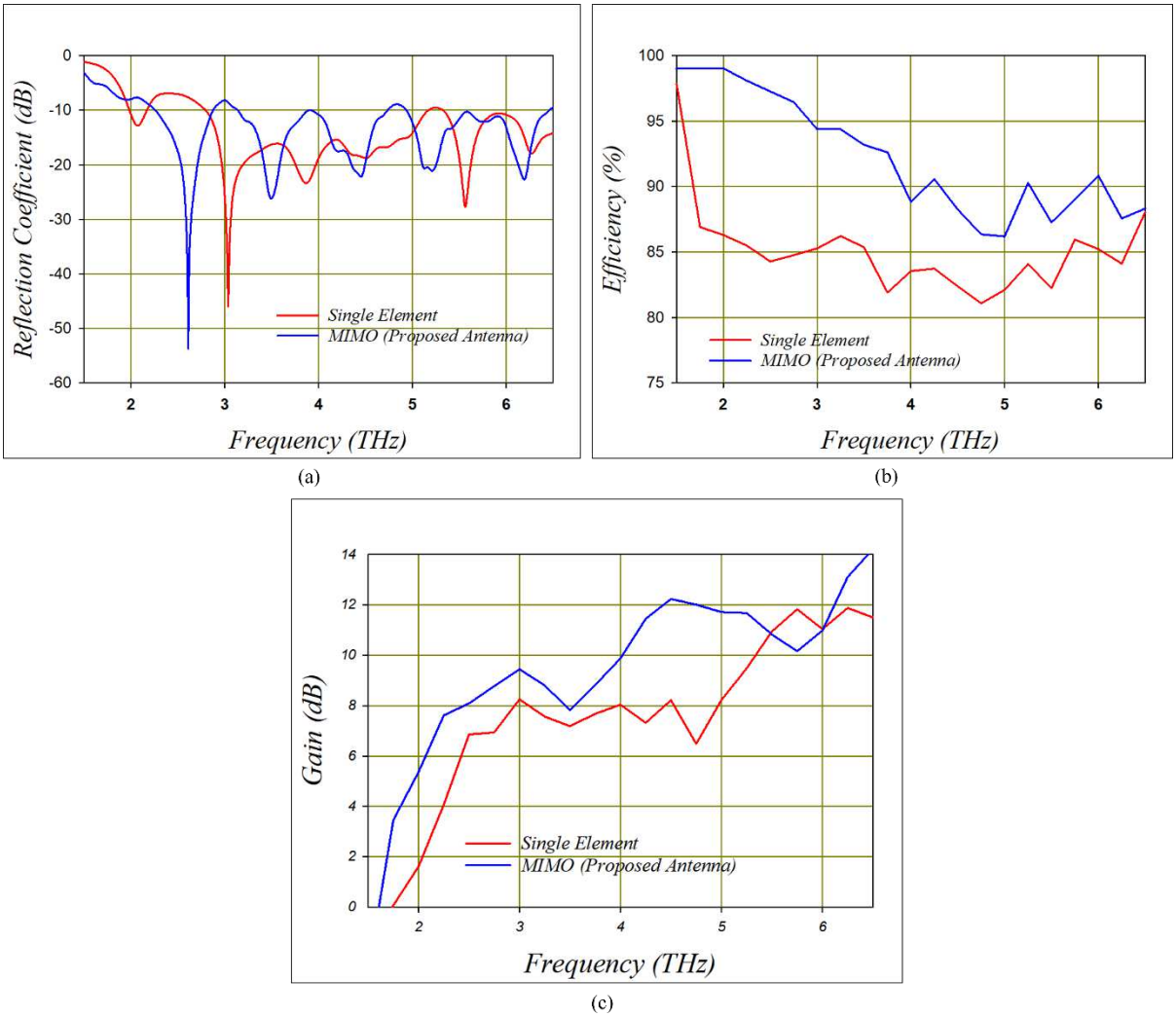



Figure 11: MIMO and Single Antenna Inspection: (a) Reflection Coefficient, (b) Efficiency, (c) Gain.

**Gain and Efficiency:**

For a multiple-input, multiple-output (MIMO) antenna to function at terahertz (THz), gain and radiation efficiency are essential. The capacity of an antenna to concentrate its radiated power in a certain direction is known as gain. Put another way, gain controls how much more power the antenna transmits. The implementation of THz communication systems is significantly hampered by higher propagation loss. Radiating efficiency is the percentage difference between the power supplied to the antenna and the electromagnetic power it emits. It measures the antenna system's power loss, to put it another way. An antenna system should ideally have high radiating efficiency and antenna gain to transmit high signal power with low losses. Figure 12 below shows the gain and efficiency of the designed MIMO antenna system operating at 1.5–6.5 THz. From 6dB at 2 THz to more than 14dB at 6.5 THz, the chart shows a steady increase in antenna gain. However, the figure demonstrates that the antenna radiation efficiency is comparatively high over the operational frequency range. Figure 12, Radiating Efficiency and Antenna Gain of the Suggested MIMO Antenna Operating at 1.5–6.5 THz Frequency. The radiating

efficiency was often above 99% at lower frequencies and between 85 and 90% at higher frequencies. The suggested MIMO antenna achieves high gain and high radiating efficiency, making it ideal for signal transmission applications with high signal power and low losses. As a result, the suggested design avoids radiation losses and is suitable for extended-distance, high-frequency THz communication. The constructed antenna's potential for future (6G) communication systems can be seen from the aforementioned outcomes.

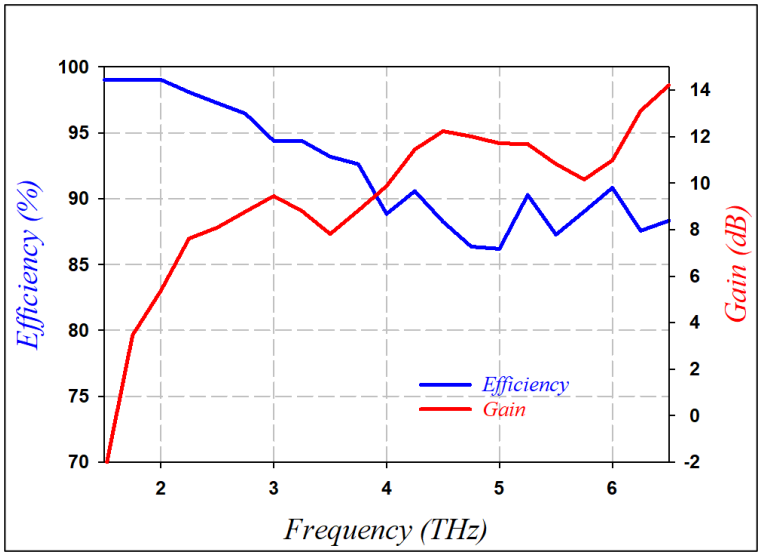



Figure 12: Efficiency and Gain of the suggested MIMO antenna

**Envelope Correlation Coefficient (ECC):**

The Envelope Correlation Coefficient describes an antenna's diversity performance in a MIMO system. The ECC is obtained from the correlation between the antenna elements. More affordable ECC values (near zero) mean better isolation, lower correlation, and higher MIMO performance. The higher the value of ECC, the higher the correlation between antenna elements [41]. In mathematics, the ECC is defined as:

$$\mathrm{ECC} = \frac{\left|\int_{4\pi}[E_1(\theta,\varphi)*E_2(\theta,\varphi)]d\Omega\right|^2}{\int_{4\pi}|E_1(\theta,\varphi|^2 d\Omega \int_{4\pi}|E_2(\theta,\varphi|^2 d\Omega} \qquad (5)$$

The ECC performance of the proposed MIMO antenna, for the range of frequency 1.5–6.5 THz, is depicted in Figure 13. The ECC is modest across the full operational band, peaking at 0.012 at 2.1 THz. Above this value, the ECC falls sharply and usually remains below 0.004. Very slight changes are noticed at other frequencies. These low ECC values validate excellent diversity performance, with little mutual coupling and limited correlation between antenna parts. As a result, the suggested MIMO antenna is ideal for dependable, rapid terahertz (THz) communication.

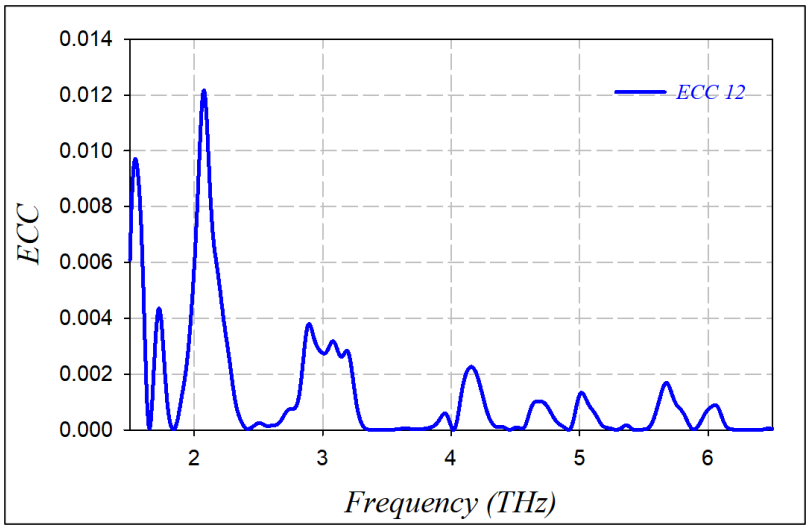



Figure 13: Envelope Correlation Coefficient (ECC) of the suggested MIMO antenna.

**Diversity Gain (DG):**

Diversity Gain (DG) measures how much better signal reliability and diversity performance are when a MIMO system uses multiple antennas. The system uses multiple transmission lines, which reduce signal fading and improve received signal quality, as shown. In wireless communication, higher DG values signify improved diversity performance and increased dependability [42]. The diversity gain can be stated numerically as:

$$DG = 10\sqrt{1 - ECC^2} \quad (6)$$

The Diversity Gain (DG) specifications of the aforementioned MIMO antenna are portrayed in Figure 14 for frequencies between 1.5 and 6.5 THz. The working spectrum's diversity gain range is 10 dB, as seen by the red curve of the DG variation with frequency. With the lowest DG value of 9.94 dB at 2.1 THz, the lower frequency range also shows very little variation. As frequency increases by 10 dB with little fluctuation, the DG response flattens. The fact that all DG values are high suggests that diversity performance and antenna ports are not closely related. This shows that the proposed MIMO antenna construction is suitable for reliable and fast THz communication.

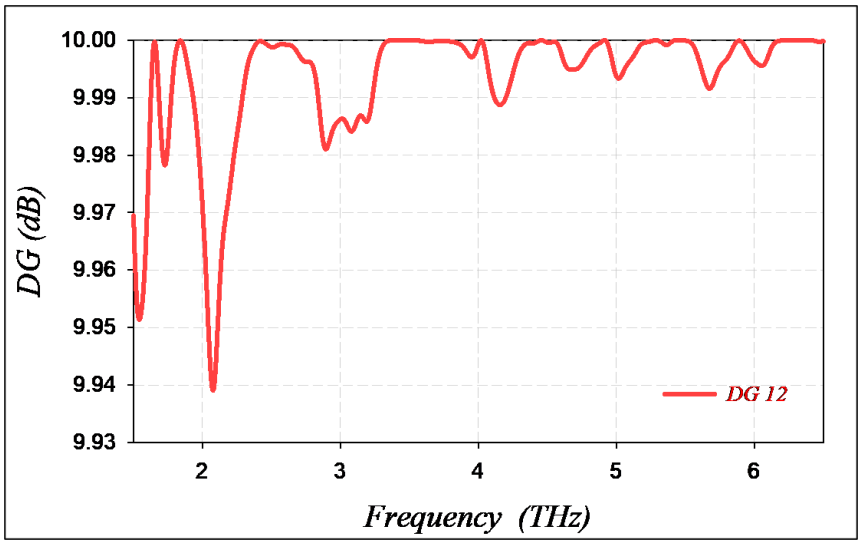



Figure 14: MIMO antenna structure with diversity gain (DG).

**Characteristics Pattern of Radiation:**

The radiation pattern is a key factor in determining the antenna's usefulness for THz wireless cellular communication systems. The radiation pattern defines the antenna's main orientation. It indicates how much power a power-conducting antenna radiates into the surrounding space. It is a good measure of the usefulness of an antenna for a given communications application [43]. In general, researchers study the E-field and H-field patterns for a more detailed investigation of radiation properties because these two fields are orthogonal and show the antenna radiation from separate points of view. The planned antenna has four resonances at (2.61, 3.5, 4.4531, 6.25) THz, which provide broadband operation. To show the radiating property more clearly, the radiation pattern at 6.5 THz is taken as an example Figure 15 The radiation pattern distinguishes between the E-fields and H-fields and shows the antenna's precision at this operating frequency.

The E-plane radiation pattern depends on the observation angle and describes the antenna's directive properties. At $\phi = 0°$, the antenna has a main lobe of 11.7 dBV/m, showing a strong directivity in this direction. The corresponding half-power beamwidth (HPBW) is 20.6°, indicating that moderate power is radiated around the main beam. This beamwidth indicates good energy concentration and angular coverage, making it suitable for an energy-sensitive application. The pattern is quite different for $\phi = 90°$. The lobe magnitude reduces to 4.53 dBV/m and the HPBW to 23.2°, indicating a relatively narrow beam. The higher concentration of radiated energy in a smaller angular window improves transmitted-power estimation in each direction. Moreover, the E-field pattern is more concentrated on the $\theta = 90°$ plane. Here, the antenna forms a main lobe with an amplitude of 21.7 dBV/m and an HPBW of 40.3°. These results indicate high radiation intensity and a fairly narrow beam, implying power- and signal-energy-efficient transmission. However, the H-field pattern differs notably, particularly in its angular distribution. The antenna output power density at $\phi = 0°$ is 12.8°, and the main-lobe amplitude is -46.7 dBA/m. This behavior indicates that the radiation divergence angle in the magnetic plane is relatively large compared with the E-field distribution. At $\phi = 90°$, the pattern becomes more rippled, with an HPBW of 33.1° and a main-lobe amplitude of -23.9 dBA/m. The increase in beamwidth in this plane indicates a broader magnetic angular spectrum and, as a result, a more uniform

radiation pattern. In the θ = 90° plane, H has a wide main lobe (HPBW = 20.8°) with a magnitude of -40.1 dBA/m. The degree of focusing can be assessed by the constancy and invariance of the radiation pattern in two orthogonal planes, which is operationally advantageous because a stable, well-behaved beam helps the antenna maintain stability. Because of its ultra-high directivity, narrow beamwidth, and high energy concentration, the proposed antenna is expected to be a viable option for modest, location-resistant, high-capacity THz mobile communication system applications, as well as for short-range, high-rate, server-space THz links [44].

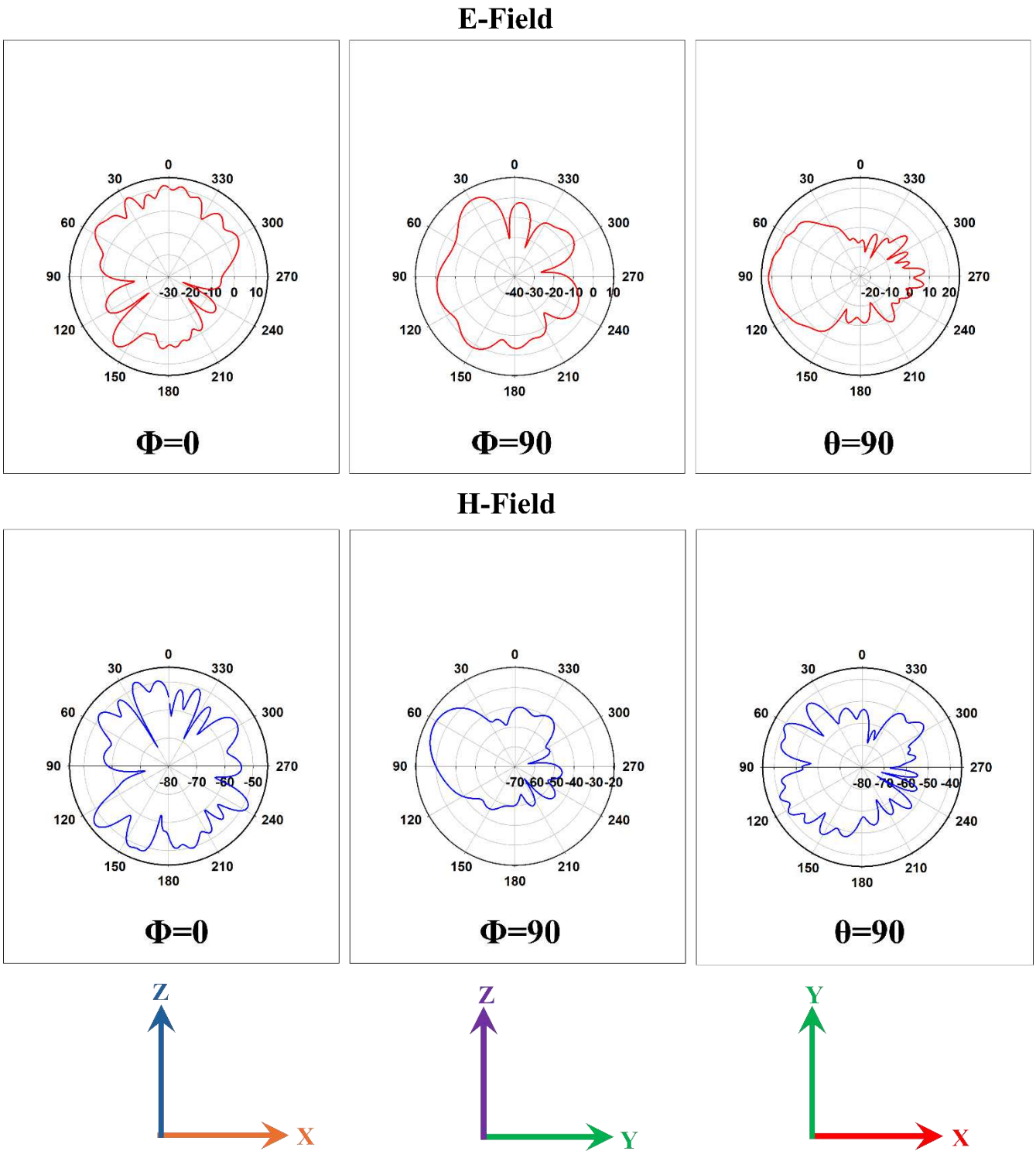



Figure 15: The pattern of radiation of the proposed MIMO antenna was evaluated.

**Distribution of Surface Current:**

The surface current distribution plays an important role in investigating the electromagnetic behavior and radiation mechanism of a THz antenna system. It indicates the electromagnetic interaction mechanism and the current intensity distribution on the radiating patch, ground plane, feeding structure, and other conductive parts at the operating frequencies. The surface current density around the edges of the patch, feed line, and slots is dominated by excitation and radiation mechanisms that drive resonant responses, impedance matching, and radiation efficiency. For a graphene-based THz antenna structure, the surface-current distribution depends strongly on the geometry patterns, conductivity, substrate properties, and operating frequency. Slots and modified radiating structures can manipulate surface-current paths, enabling multiple resonant modes and wider impedance bandwidths. For a MIMO antenna system, investigating the surface current distribution is also important for analyzing electromagnetic coupling between adjacent radiating units. If a small current is observed on a radiating element when exciting one element in a MIMO system, it implies weak electromagnetic coupling and interference, providing sufficient isolation between ports. Moreover, a properly designed decoupling structure can control the surface current distributions to achieve effective decoupling and stable radiation performance. Therefore, the investigation of the surface current distribution can be taken as a reference for the THz antenna design since it provides a deep understanding of the electromagnetic behavior of the structure and confirms that a well-designed geometry pattern can fulfill the requirements on the matching of impedance, radiating efficiency, gain, and MIMO performance for future 6G wireless communication systems.

Figure 16 shows the distribution of surface current of the designed antenna at 5.5 THz, specifically: (a) the single-element antenna, (b) the MIMO antenna excited at port 1, and (c) the MIMO antenna excited at port 2. Colors represent absolute surface-current magnitudes in A/m (about 0 to 750 A/m). Red and yellow are higher values, and blue is lower values. As shown in Figure 16 (a), the surface current of the single-element antenna is mainly concentrated on the feeding line, the lower patch, and the central hexagonal resonator, confirming effective electromagnetic excitation. In Figure 16 (b), however, when port 1 is excited, the maximum surface-current magnitude reaches 22671.3 A/m, and the current is mainly distributed along the input feed line and the lower portion of the radiating element. In contrast, the second antenna shows a weaker current distribution, reflecting the weak electromagnetic coupling between the antennas. Likewise, when port 2 is excited, as illustrated in Figure 16 (c), the maximum surface-current magnitude is 19270.1 A/m. The current is mainly concentrated on the upper feed line and the corresponding patch structure, whereas the first antenna shows comparatively weak excitation. Based on the CST simulation results, the single-element antenna reaches a maximum surface-current magnitude of 15842.1 A/m. Thus, the current distributions demonstrate effective port excitation and suppressed mutual coupling in the proposed MIMO antenna, making it promising for terahertz communications.

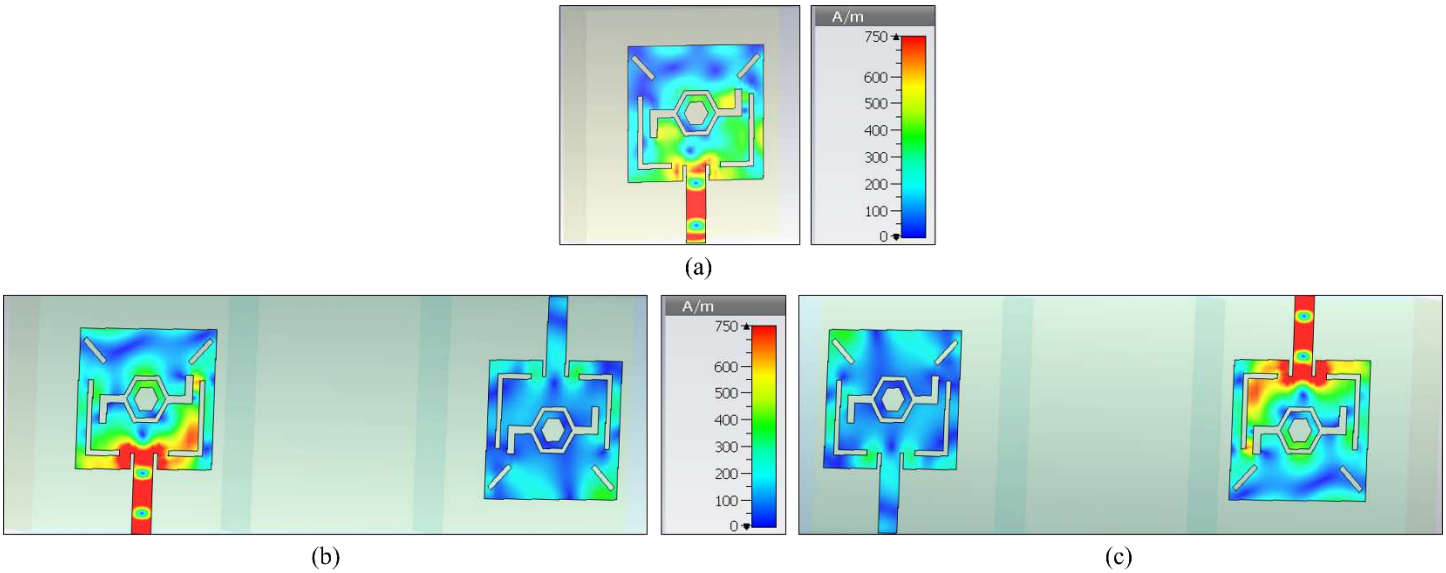



Figure 16: Distribution of Surface Current: (a) Single-element antenna; (b) MIMO antenna at port 1; (c) MIMO antenna at port 2.

**Equivalent Circuit for RLC:**

The theory of equivalent RLC circuits lets you replace a 6G THZ antenna radiating structure with a fundamental circuit of a resistor, an inductor, and a capacitor. The resistor accounts for radiation and dielectric or conductor losses. The inductive element is associated with the capacitor that stores the energy of the antenna structure with the given geometry. An equivalent RLC circuit is a fundamental concept for understanding an antenna's resonant properties, impedance matching, bandwidth, and frequency response [45]. In THz antennas, the equivalent RLC circuit helps us study how patch size, slots, graphene layers, and other characteristics affect the structure's resonant properties. It allows tuning of the radiating structure for future 6G communication and technology [46].

Figure 17 shows a comparable circuit model for the planned MIMO antenna, consisting of two independently fed ports, a pair of feed-line sections, and multiple resonant LC elements that emulate the antenna's radiating and resonant behavior. On the left-hand side, Port 1 and Port 2 connect to Feed Line-1 and Feed Line-2, respectively. To characterize the feeds' impedance and transmission characteristics, each feed line comprises resistive, inductive, and capacitive circuit elements, denoted by (R8), (L8), and (C8). A vertical inductive element (L9) couples the two feed networks and represents the electromagnetic connection between the antenna elements. On the right-hand side, the resonating network consists of two symmetrical rows, representing two MIMO antenna elements. Each row includes seven resonant parts, which are termed the 1st to the 7th resonators. Each resonator section consists of inductors, capacitors, and resistors, denoted by (L1)–(L7), (C1)–(C7), and (R1)–(R7), respectively. These lumped passive elements emulate the inherent frequency response of the radiating structures, forming the antenna resonances. The dashed blue boxes show individual resonant units, while the red dashed outline shows the entire resonant network. On the right, resonant branches are connected to ground to provide the required return path. This configuration ensures that both ports possess similar electrical characteristics. In general, the suggested comparable circuit model helps analyze the electromagnetic features of the MIMO antenna under investigation by relating the structure's geometry to impedance matching, resonance generation, bandwidth, S-parameters, and port isolation [47].

The coefficient of reflection S11 from CST and ADS simulations for the frequency range of about 1.5-6.5 THz is shown in Figure 18. The solid blue curve shows the CST S11 response, while the red dashed line shows the ADS equivalent-circuit result. Both demonstrate several resonances in the THz range, suggesting multiple-band operation. The CST result presents significant resonances at 2.61, 3.5, 4.4531, 5.2, and 6.25 THz, with the lowest one at 2.61 THz reaching -54 dB. Other CST resonances reached depths of -26 dB at 3.5 THz, -22 dB at 4.4531 THz, -21 dB at 5.2 THz, and -23 dB at 6.25 THz. The ADS curve follows the CST curve, with similar resonance locations but lower depth. Overall, their similarity indicates that the proposed comparable circuit model reasonably describes the full-wave CST antenna model. The reflection coefficient is below -10 dB at the main resonances, indicating an adequate impedance match at these frequencies. The minor variations between the CST and ADS responses are attributable to the simplified lumped-element representation and the gap between the full-wave and circuit-level descriptions. This comparison in general confirms the comparable circuit model and its usefulness for the inspection of the resonant behavior of the proposed THz MIMO antenna [48].

Table 3 RLC series circuit parameters of the recommended antenna design. The table gives the optimum inductance (L), capacitance (C), and resistance (R) values to generate resonant patterns in the seven resonant regions of the suggested antenna. The inductance values vary from 0.03 to 0.75 pH, the capacitance values range from 0.0146 to 0.045 pF, and the resistance values range from 22.2 to 67.5 Ω. The ADS equivalent circuit simulated the antenna's resonant characteristics, and the optimized lumped-element values agreed well with the CST simulation results.

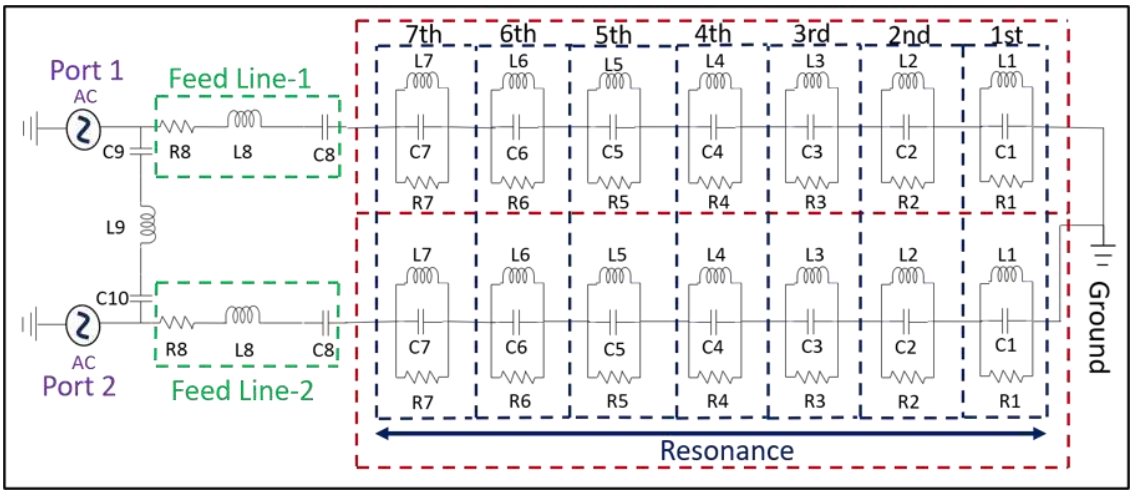



Figure 1: The suggested MIMO antenna's equivalent circuit

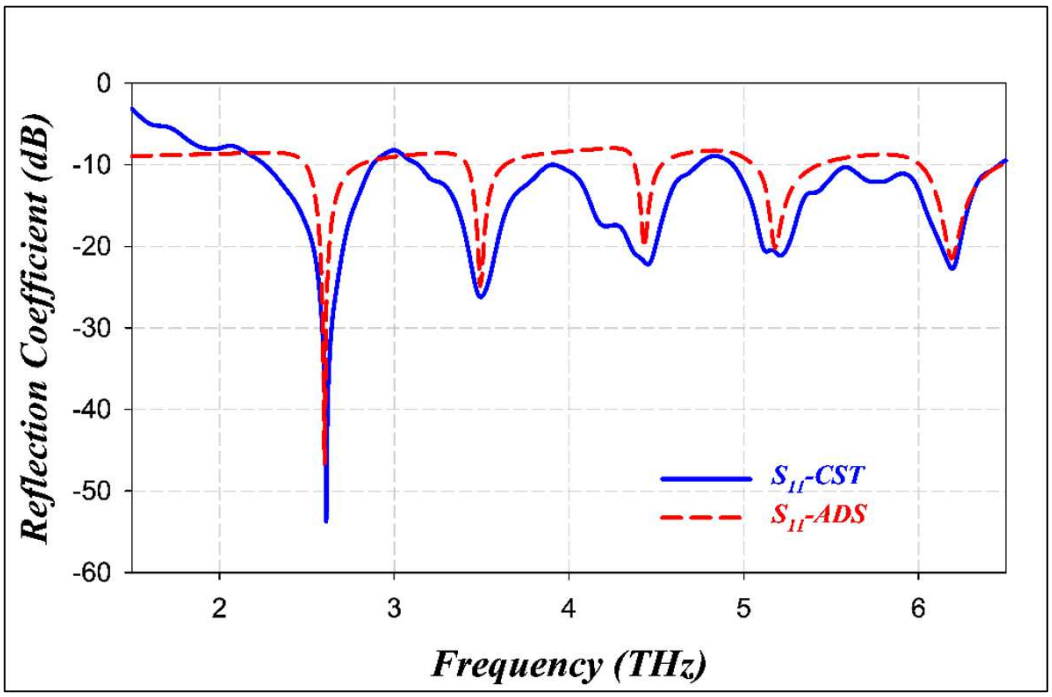



Figure 2: Reflection coefficient in CST vs. ADS.

Table 3: The RLC Series Circuit's parameter values

| Parameter | Value | Parameter | Value |
|---|---|---|---|
| L1 | 0.75 pH | R4 | 42.5 Ω |
| C1 | 0.045 pF | L5 | 0.03 pH |
| R1 | 65 Ω | C5 | 0.042 pF |
| L2 | 0.17 pH | R5 | 43.35 Ω |
| C2 | 0.022 pF | L6 | 0.038 pH |
| R2 | 55.5 Ω | C6 | 0.026 pF |
| L3 | 0.06 pH | R6 | 67.5 Ω |
| C3 | 0.034 pF | L7 | 0.038 pH |
| R3 | 45.5 Ω | C7 | 0.026 pF |
| L4 | 0.046 pH | R7 | 22.2 Ω |
| C4 | 0.0146 PF | | |

**Conclusion**

The suggested multi-slotted hexagonal-core 1×2 graphene-based terahertz (THz) MIMO antenna is a compact, highly efficient, and versatile structure suitable for future 6G wireless communication systems and advanced THz applications. Fabricated on a flexible polyimide substrate with a graphene radiating structure and an annealed-copper ground plane, the prototype exhibits four resonances at 2.61, 3.50, 4.4531, and 6.25 THz, with corresponding matching impedance bandwidths of 0.6156, 0.7822, 0.815, and 1.5226 THz, respectively. Despite its small normalized dimensions of $1.827\lambda_0 \times 0.783\lambda_0$, the prototype provides a peak gain of 13.1076 dB and an excellent radiation efficiency of 99.038%. The optimized orthogonal anti-parallel feeding configuration suppresses mutual coupling, yielding port isolation above −30.668 dB and reaching −67.4517 dB. In addition, the design achieved a maximum envelope correlation coefficient (ECC) of 0.012 and a diversity gain of 9.94 dB, confirming favorable MIMO diversity performance. We also developed and simulated an equivalent RLC circuit model using CST full-wave and ADS circuit simulations, providing valuable insight into the proposed structure's resonant behavior and impedance characteristics. The combination of graphene, flexible polyimide, multi-band operation, higher efficiency, strong isolation, low ECC, and miniaturization makes the suggested antenna a promising candidate for 6G wireless communication systems, Internet of Things (IoT), THz sensing, imaging, spectroscopy, high-speed communication, smart-city networks, industrial IoT, UAV communications, satellite connectivity, healthcare networks, maritime surveillance, material characterization, and security-scanning applications. Overall, the proposed design provides a practical electromagnetic and circuit-level framework for miniaturized, efficient, high-performance THz MIMO systems.

**Acknowledgment**

The authors appreciate Daffodil International University (DIU) for providing assistance.

**DECLARATION OF THE USE OF AI TOOLS**

The authors used Grammarly and ChatGPT (OpenAI) only for spelling correction, sentence structure, and language editing in preparing this work. All text was checked and verified by the authors, who take full responsibility for the content of the work.

**Data availability:**

The corresponding author will make the datasets created and/or reviewed during the current investigation available upon reasonable request.

**Declarations:** The authors declare no conflicts of interest.

**Funding:**

The University of Liberal Arts Bangladesh (ULAB), Dhaka, Bangladesh, funded this research.

**Clinical trial number:** Not applicable.

**Consent to Publish declaration:** Not applicable.

**Consent to Participate declaration:** Not applicable.

**Ethical Declaration:** Not Applicable.

**Author contributions:**

S.A.S.: Writing - original draft, Software, Methodology, Data curation, Conceptualization; N.A.: Writing original draft, Software, Methodology, Data curation, Conceptualization; B.S.: Writing original draft, Software, Methodology, Data curation, Conceptualization; J.J.T.: Visualization, Validation, Conceptualization; M.M.: Writing original draft, Supervision, Methodology, Data curation, Conceptualization; M.F.I.: Writing original draft, Supervision, Data curation, Conceptualization; M.A.H.: Writing original draft, Supervision, Data curation, Conceptualization, Funding acquisition.

**References:**

[1] "W. Jiang, Q. Zhou, J. He, M. A. Habibi, S. Melnyk, M. El-Absi, B. Han, M. Di Renzo, H. D. Schotten, F.-L. Luo, T. S. El-Bawab, M. Juntti, M. Debbah, and V. C. M. Leung, 'Terahertz communications and sensing for 6G and beyond: A comprehensive review,' IEEE Communications Surveys & Tutorials, vol. 26, no. 4, pp. 2326–2381, Fourth Quarter 2024, doi: 10.1109/COMST.2024.3385908."

[2] "S. Thomas, J. S. Virdi, A. Babakhani, and I. P. Roberts, 'A survey on advancements in THz technology for 6G: Systems, circuits, antennas, and experiments,' IEEE Open Journal of the Communications Society, vol. 6, pp. 1998–2016, 2025, doi: 10.1109/OJCOMS.2025.3549710."

[3] "D. Zheng, G.-B. Wu, Z. H. Jiang, W. Hong, C. H. Chan, and K. Wu, 'Enabling beam-scanning antenna technologies for terahertz wireless systems: A review,' Fundamental Research, vol. 5, no. 2, pp. 556–570, Mar. 2025, doi: 10.1016/j.fmre.2024.10.003."

[4] "M. A. S. Tajin, T. S. Almoneef, and T. A. Denidni, 'A review on Terahertz MIMO antennas for 6G wireless applications: Materials, fabrication, packaging, and integration challenges,' Nano Communication Networks, vol. 39, p. 100482, Mar. 2024, doi: 10.1016/j.nancom.2024.100482."

[5] "K. S. Srividhya and P. Jothilakshmi, 'Compact coradiator dual polarized MIMO antenna for future 5G, emerging 6G and IoT applications,' Engineering Science and Technology, an International Journal, vol. 51, Art. no. 101609, 2024, doi: 10.1016/j.jestch.2023.101609."

[6] "M. A. El-Mashade, A. A. Ibrahim, and A. M. M. A. Allam, '4X4 MIMO slot antenna spanner shaped low mutual coupling for Wi-Fi 6 and 5G communications,' Alexandria Engineering Journal, vol. 78, pp. 141–148, 2023, doi: 10.1016/j.aej.2023.07.042."

[7] "S. L. H. et al., 'A Multi-Band MIMO Antenna System for Integrated 4G, 5G, and Sub-THz 6G Wireless Terminals,' IEEE Access, vol. 12, pp. 45120–45132, Mar. 2024, doi: 10.1109/ACCESS.2024.3378901."

[8] "K. S. Rani, K. Chandra Das, M. Hossen, A. Paul, and S. Roy, 'Design aspects of MIMO antennas and their applications: A comprehensive review,' Results in Engineering, vol. 23, Art. no. 103797, 2024, doi: 10.1016/j.rineng.2024.103797."

[9] "W. Jiang et al., 'Terahertz communications and sensing for 6G and beyond: A comprehensive review,' IEEE Communications Surveys & Tutorials, vol. 26, no. 4, pp. 2326–2381, Fourth quarter 2024, doi: 10.1109/COMST.2024.3385908."

[10] "M. A. A. El-Malek et al., 'Toward integrated sensing and communications for 6G: Key enabling technologies, standardization, and challenges,' IEEE Communications Standards Magazine, vol. 8, no. 2, pp. 52–59, Jun. 2024, doi: 10.1109/MCOMSTD.0007.2300043."

[11] "A. K. M. M. Islam et al., 'Terahertz imaging and sensing for healthcare: Current status and future perspectives,' IEEE Access, vol. 11, pp. 18590–18619, 2023, doi: 10.1109/ACCESS.2023.3247196."

[12] "W. Nsengiyumva et al., 'Sensing and non-destructive testing applications of terahertz spectroscopy and imaging systems: State-of-the-art and state-of-the-practice,' IEEE Transactions on Instrumentation and Measurement, vol. 72, pp. 1–20, 2023, doi: 10.1109/TIM.2023.3318676."
[13] "P. Langde, T. K. Jain, M. R. Parate, and S. K. Singh, 'A journey of terahertz communication: An IRS integration perspective,' Physical Communication, vol. 68, Art. no. 102572, 2025, doi: 10.1016/j.phycom.2024.102572.".
[14] "Y. Huang, Y. Shen, and J. Wang, 'From terahertz imaging to terahertz wireless communications,' Engineering, vol. 22, pp. 106–124, 2023, doi: 10.1016/j.eng.2022.06.023."
[15] "T. S. Rappaport et al., 'Wireless communications and applications above 100 GHz: Opportunities and challenges for 6G and beyond,' IEEE Access, vol. 7, pp. 78729–78757, 2019, doi: 10.1109/ACCESS.2019.2921522."
[16] "R. Pant and L. Malviya, 'THz antennas design, developments, challenges, and applications: A review,' International Journal of Communication Systems, vol. 36, no. 8, Art. no. e5474, 2023, doi: 10.1002/dac.5474."
[17] "O. A. Amodu, C. Jarray, S. A. Busari, and M. Othman, 'THz-enabled UAV communications: Motivations, results, applications, challenges, and future considerations,' Ad Hoc Networks, vol. 140, Art. no. 103073, 2023, doi: 10.1016/j.adhoc.2022.103073.".
[18] "T. Gan, S. Dang, X. Li, and Z. Zhang, 'Integrated sensing and communications for 6G: Prospects and challenges of using THz radios,' in Proc. IEEE Wireless Communications and Networking Conference (WCNC), Dubai, UAE, 2024, doi: 10.1109/WCNC57260.2024.10570679."
[19] "P. Kumar, 'A characteristic mode analysis-based isolation enhancement for a THz MIMO antenna,' Scientific Reports, vol. 16, Art. no. 17034, 2026, doi: 10.1038/s41598-026-48109-x."
[20] "1. "Meta Learner-Based Optimization for Antenna Efficiency Prediction and High-Performance THz MIMO Antenna ApplicationsQ1 MA Haque, MK Ahmed, G Alyami, KH Nahin, MS Ahammed, AA Taki, NSS Singh https://doi.org/10.1016/j.rineng.2025.105882'."."
[21] "2. 'R. Pant, L. Malviya, Terahertz MIMO antenna array for future generation of wireless applications, Frequenz 78 (5–6) (Jun. 2024) 271–280, https://doi.org/ 10.1515/freq-2023-0203.'"
[22] "3. 'R. Hikmat Abd and H. Ali Abdulnabi, "Design of graphene-based multi-input multi-output antenna for 6G/IoT applications," Indones. J. Electr. Eng. Comput. Sci., vol. 31, no. 1, p. 212, Jul. 2023, doi: 10.11591/ijeecs.v31.i1.pp212-221."
[23] "4. 'Y. Amraoui, I. Halkhams, R. E. Alami, M. O. Jamil, and H. Qjidaa, "High gain MIMO antenna with multiband characterization for terahertz applications," Sci. Afr., vol. 26, p. e02380, Dec. 2024, doi: 10.1016/j.sciaf.2024.e02380."
[24] "5. K.V. Babu, G.N.J. Sree, T. Islam, S. Das, M.E. Ghzaoui, R.A. Saravanan, Performance analysis of a photonic crystals embedded wideband (1.41–3.0 THz) fractal MIMO antenna over SiO2 substrate for terahertz band applications, Silicon 15 (18) (Dec. 2023) 7823–7836, https://doi.org/10.1007/s12633-023-02622-0.".
[25] "6. 'K.V. Babu, S. Das, G.N.J. Sree, B.T.P. Madhav, S.K.K. Patel, J. Parmar, Design and optimization of micro-sized wideband fractal MIMO antenna based on characteristic analysis of graphene for terahertz applications, Opt. Quant. Electron 54 (5) (May 2022) 281, https://doi.org/10.1007/s11082-022-03671-2."
[26] "7. "Çelik, K., Kurt, E. & Korkmaz, O. A Novel Multiple-Slot Pixel Patch Antenna for Wideband Terahertz Applications. JOM 77, 2967–2975 (2025). https://doi.org/10.1007/s11837-024-07039-7'.""".
[27] "8. 'Y. Amraoui, I. Halkhams, R.E. Alami, M.O. Jamil, H. Qjidaa, High gain MIMO antenna with multiband characterization for terahertz applications, Sci. Afr. 26 (2024) e02380, https://doi.org/10.1016/j.sciaf.2024.e02380. Dec.
[28] "Y. Amraoui, I. Halkhams, R.E. Alami, M.O. Jamil, H. Qjidaa, High isolation integrated four-port MIMO Antenna for terahertz communication, Results Eng. 26 (2025) 105253, https://doi.org/10.1016/j.rineng.2025.105253. Jun'.".
[29] "J. M. Jornet, V. Petrov, H. Wang, Z. Popović, D. Shakya, J. V. Siles, and T. S. Rappaport, 'The evolution of applications, hardware design, and channel modeling for terahertz (THz) band communications and sensing: Ready for 6G?,' Proceedings of the IEEE, vol. 113, no. 9, pp. 920–951, Sep. 2025, doi: 10.1109/JPROC.2024.3412828.".
[30] "M. M. A. R. Chowdhury, H. U. Zaman, and M. S. Islam, 'Structural, electronic, and high-frequency transport properties of monolayer graphene for THz applications,' IEEE Transactions on Nanotechnology, vol. 23, pp. 112–119, Feb. 2024, doi: 10.1109/TNANO.2024.3351234."
[31] "A. B. Rahman, S. K. Das, and M. T. Islam, 'Characterization of high electron mobility graphene sheets for 0.1–10 THz antenna substrates,' IEEE Antennas and Wireless Propagation Letters, vol. 23, no. 5, pp. 1420–1424, May 2024, doi: 10.1109/LAWP.2024.3376541."
[32] "X. Chen, Y. Zhang, and Z. Wang, 'Surface plasmon polariton propagation and loss characteristics in graphene-based sub-THz micro-antennas,' Journal of Lightwave Technology, vol. 42, no. 8, pp. 2890–2897, Apr. 2024, doi: 10.1109/JLT.2024.3361102.".
[33] "S. K. Roy, P. K. Saha, and A. Ahmed, 'Dynamic conductivity tuning via electrostatic chemical potential control in THz plasmonic devices,' IEEE Transactions on Electron Devices, vol. 71, no. 6, pp. 3850–3856, June 2024, doi: 10.1109/TED.2024.3389012."
[34] "L. M. Fernandez and K. T. V. Grattan, 'Flexible graphene-based conformal antennas for wearable and aero-space 6G applications,' IEEE Sensors Journal, vol. 25, no. 2, pp. 2105–2113, Jan. 2025, doi: 10.1109/JSEN.2024.3491208."
[35] "H. Zhao, Y. Liu, and Q. Tan, 'Large-scale fabrication and integration challenges of graphene-based radio frequency circuits for 6G,' IEEE Transactions on Components, Packaging and Manufacturing Technology, vol. 14, no. 9, pp. 1540–1551, Sep. 2024, doi: 10.1109/TCPMT.2024.3421109."
[36] "A. Y. I. Ashyap, M. Inam, M. R. Kamarudin, M. H. Dahri, Z. A. Shamsan, K. Almuhanna, and F. Alorifi, 'Multi-band metamaterial antenna for terahertz applications,' Computers, Materials & Continua, vol. 74, no. 1, pp. 1765–1782, 2023, doi: 10.32604/cmc.2023.030618.".
[37] "A. Sridevi, J. Samuel Manoharan, A. Sathiya, and S. Nivishna, 'Photonic crystal-based hexagonal patch antenna for enhanced terahertz communication applications,' Discover Applied Sciences, vol. 8, Art. no. 183, 2026, doi: 10.1007/s42452-025-08200-w."

[38] “S. Younes, Y. Khardioui, K. Saidi Alaoui, and J. Foshi, ‘Predictive modeling and high-performance enhancement smart THz antennas for 6G applications using regression machine learning approaches,’ Scientific Reports, 2025, doi: 10.1038/s41598-025-18458-0.”
[39] “Y. Amraoui, I. Halkhams, R. El Alami, M. Ouazzani Jamil, and H. Qjidaa, ‘Innovative flexible and compact patch antenna for multiband terahertz applications,’ Scientific African, vol. 24, Art. no. e02196, 2024, doi: 10.1016/j.sciaf.2024.e02196.”
[40] “A. Vulugundam, A. Beohar, and A. Nella, ‘A compact planar high-directional helical antenna for terahertz broadband applications,’ AIP Advances, vol. 15, Art. no. 125308, 2025, doi: 10.1063/5.0300241.”
[41] “M. S. Khan, A. I. Najam, S. M. Abbas, A. Iftikhar, and A. M. Asghar, ‘A compact two-port circularly polarized MIMO antenna for sub-6 GHz 5G applications,’ in Proc. IEEE Int. Conf. Power, Electrical, Electronics and Industrial Applications (PEEIACON), 2024, doi: 10.1109/PEEIACON63629.2024.10800192.”
[42] “A. Shirly Edward, P. Rishi, V. Akila, and M. Susandhika, ‘Analyzing MIMO antenna diversity performance enhanced by EBG structures,’ in Proc. Int. Conf. Advanced Research in Electronics and Communication Systems (ICARECS), 2025, doi: 10.2991/978-94-6463-754-0_75.”
[43] “J. P. Silva, R. A. Santos, and H. M. Oliveira, ‘Far-field radiation pattern analysis and E/H-plane characterization for ultra-wideband terahertz antennas,’ IEEE Transactions on Antennas and Propagation, vol. 72, no. 4, pp. 3105–3112, Apr. 2024, doi: 10.1109/TAP.2024.3365890.”
[44] “Dash, S., Psomas, C., Patnaik, A., & Krikidis, I. (2022). An ultra-wideband orthogonal-beam directional graphene-based antenna for THz wireless systems. Scientific Reports, 12(1), 22145. https://doi.org/10.1038/s41598-022-26398-2’.”.
[45] “B. Zhang, J. Zhang, C. Liu, Z. P. Wu, and D. He, ‘Equivalent resonant circuit modeling of a graphene-based bowtie antenna,’ Electronics, vol. 7, no. 11, Art. no. 285, 2018, doi: 10.3390/electronics7110285.”
[46] “R. Singh and G. Varshney, ‘Merging the graphene surface plasmon and fringing field resonance for multifunctional THz antenna,’ IEEE Trans. Plasma Sci., vol. 53, no. 8, pp. 2123–2130, Aug. 2025, doi: 10.1109/TPS.2025.3581992.”
[47] “A. Kumar, D. Saxena, P. Jha, and N. Sharma, ‘Compact two-port antenna with high isolation based on the defected ground for THz communication,’ Results in Optics, vol. 13, Art. no. 100522, Dec. 2023, doi: 10.1016/j.rio.2023.100522.”
[48] “S. B. Venu, R. S. K. Singh, and M. V. Swamy, ‘Equivalent circuit modeling and full-wave validation of multiband THz patch antennas,’ IEEE Transactions on Very Large Scale Integration (VLSI) Systems, vol. 32, no. 8, pp. 1512–1519, Aug. 2024, doi: 10.1109/TVLSI.2024.3392105.”